Electron-Nuclear Interaction in Antimony Metal*†

E. H. Hygh‡ and T. P. Das
Department of Physics, University of California, Riverside, California
(Received 4 June 1965; revised manuscript received 6 October 1965)

The field gradient at the nuclei due to the conduction electrons in antimony metal is calculated using an approximation for their wave functions in keeping with available information concerning the Fermi surface of antimony metal. It is shown that the Wannier functions for antimony can be closely approximated by a set of orthogonalized atomic orbitals (OAO) which are mixed by the noncentral terms in the one-electron Hamiltonian. The mixing of the s-like and p-like OAO is seen to be analogous to the concept of s-p hybridization in the simple chemical picture of the solid. Combined with earlier calculations of the field gradient due to the ion cores, the total field gradient comes out as $eq=1998\times10^{12}$ esu/cm^3 as compared to 1889×10^{12} esu/cm^3, the experimental value of the gradient based on Hewitt and Williams's quadrupole-resonance data and Murakawa's values of the quadrupole moments of the $Sb^{121,123}$ nuclei. In addition, we have calculated the direct contributions to the isotropic and anisotropic Knight shifts from the spins of the conduction electrons near the Fermi surface. These are found to be $\delta_{iso}=+0.07\%$ and $\delta_{ax}=-0.05\%$. It is hoped that when experimental values of these quantities become available in the future a comparison with the theoretical values of the direct contributions will permit an assessment of the importance of other contributors to the Knight shift such as core polarization and orbital effects.

I. INTRODUCTION

INFORMATION on the band structure and Fermi surface of metals can be derived by a variety of techniques[1–5] such as cyclotron resonance, anomalous skin effect and de Haas–van Alphen effect, to name only three of a number that are in extensive use currently. These measurements require for their interpretation a knowledge of the energy bands, that is, the variation of energy with momentum of the electrons. On the other hand, there are also a great variety of data obtainable from nuclear- and electron-spin-resonance measurements[6,7] and Mössbauer-effect studies.[8] These data yield such properties as the quadrupole coupling constant for the nucleus, the magnetic field produced by the electrons at the nucleus, termed the Knight shift in the literature, and the g factor for the conduction electrons. Knight-shift and quadrupole-coupling data cannot be explained from a study of the energy bands alone; they require a knowledge of the wave functions as well.[9,10]

Various analyses[11–13] of the contributions to the field gradients at the nuclei from the positive ions have clearly indicated that in most metals, the major part of the field gradient arises from the conduction electrons. The analysis[10] of the contribution to the field gradient in metallic beryllium was somewhat inconclusive because no account was taken of the departure of the Fermi-surface from a sphere and also because the quadrupole moment of Be^9 was not accurately known. The interpretation of the quadrupole-interaction data differs in nature from that of data such as de Haas–van Alphen effect, cyclotron resonance and other such measurements in two important aspects. First, it does not give directly a feature of the energy band at any part of the Fermi surface but instead serves as a detailed check of calculated band structure and wave functions. Secondly, since it involves a contribution from the charge density in real space, it requires information about the electronic wave functions over all of k space and not only near the Fermi surface. The Knight shift, at least in the lighter metals, on the other hand, requires a knowledge of the wave functions near the Fermi surface. In the light metals, the Knight shift is considered as arising from the contact interaction between the nucleus and the

* Supported by the National Science Foundation.

† Based on a thesis submitted by E. H. Hygh in partial fulfillment of the requirements for the Doctor of Philosophy degree at the University of California, Riverside, California, 1964.

‡ This work done in part while at the Infrared Division of the Research Department, U. S. Naval Ordnance Laboratory, Corona, California. Present address: Department of Physics, University of Utah, Salt Lake City, Utah.

[1] For an extensive review of cyclotron-resonance method see A. B. Pippard, *Advances in Electronics and Electron Physics* (Academic Press Inc., New York, 1954), Vol. 6, p. 1.

[2] The anomalous skin effect is treated in Ref. 1.

[3] For a complete review of the de Haas–van Alphen technique see D. Shoenberg, Phil. Trans. Roy. Soc. (London) **A245**, 1 (1952), and by A. B. Pippard, Rept. Progr. Phys. **23**, 176 (1960).

[4] The Shubnikov–de Haas effect is also presented in Ref. 2.

[5] For a treatment of the method of ultrasonic attenuation or magnetoacoustic absorption see A. B. Pippard, Proc. Roy. Soc. (London) **A257**, 165 (1960), and Rept. Progr. Phys. **23**, 176 (1960).

[6] A. Abragam, *Nuclear Magnetism* (Oxford University Press, London, 1961); W. D. Knight, in *Solid State Physics*, edited by F. Seitz and D. Turnbull (Academic Press Inc., New York, 1956), Vol. 2, p. 933; A. K. Saha and T. P. Das, *Nuclear Induction* (Saha Institute of Nuclear Physics, Calcutta, India, 1957); T. P. Das and E. L. Hahn, *Nuclear Quadrupole Resonance Spectroscopy* (Academic Press Inc., New York, 1958).

[7] W. Low, *Electron Paramagnetic Resonance* (Academic Press Inc., New York, 1958); C. P. Slichter, *Principles of Magnetic Resonance* (Harper and Row, Publishers, Inc., New York, 1963).

[8] G. Wertheim, *Mössbauer Effect: Principles and Applications* (Academic Press Inc., New York, 1964).

[9] W. D. Knight, see Ref. 6.

[10] M. Pomerantz and T. P. Das, Phys. Rev. **119**, 70 (1960).

[11] T. P. Das and M. Pomerantz, Phys. Rev. **123**, 2070 (1961).

[12] W. W. Simmons and C. P. Slichter, Phys. Rev. **121**, 1580 (1961); R. R. Hewitt and T. T. Taylor, *ibid.* **126**, 524 (1962); see also Ref. 10.

[13] D. R. Torgeson and R. G. Barnes, Phys. Rev. **136**, A738 (1964).

conduction electrons.[14] In addition, of course, one has to consider the contribution from the polarization of the core electrons by the conduction electrons.[15] The core polarization, however, still requires only a knowledge of the conduction-electron wave functions near the Fermi surface besides a knowledge of core-electron wave functions as perturbed by the nuclear magnetic moment. For the heavier metals, there seems to be convincing evidence[16] that an important role is played by the orbital motion of the conduction electrons. Such contributions to the Knight shift are evidently more difficult to calculate because, for a quantitative evaluation, they require a knowledge of not just the zero-order conduction-electron wave functions, but also their perturbed forms in the presence of a magnetic field.[17] The interpretation of the shift in the g factor of the conduction electrons also requires a knowledge of perturbed wave functions for the conduction electrons, taking into account the spin-orbit interaction.

Not much attention has been devoted in earlier calculations on metals to the study of wave functions, perhaps because of preponderance of available data from cyclotron resonance, de Haas–van Alphen, anomalous skin effect and other such measurements. But in the past few years there has been a continued development of methods for calculating band structure and wave functions in metals and alloys and an increasing availability of accurate data from resonance data. It is, therefore, worthwhile to examine whether the results of a single calculation on a metal based on one of the several different available methods can give reasonable agreement with both properties which depend on features of the energy bands and those that require a knowledge of the wave functions. Such a program has been started in our laboratory. In the present paper we shall report our calculations on the antimony metal. In subsequent papers, results of calculations currently in progress on beryllium and indium metals will be reported.

In Sec. II, we shall consider the wave functions for the conduction electrons in antimony metal. The procedure and results of calculation for the field gradient at the $Sb^{121,123}$ nuclei will be presented in Sec. III and compared with experiment.[18] In Sec. IV, the direct contributions to the isotropic and anisotropic Knight shifts will be considered. In Sec. IV, the various sources of error and the importance of other contributions to the Knight shifts and the quadrupole coupling constant will be discussed.

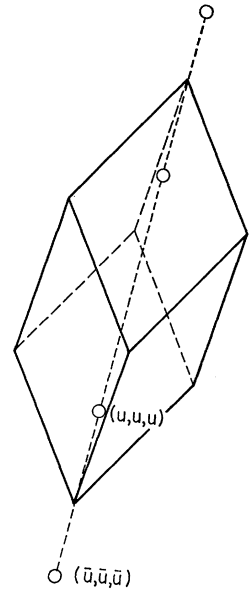

FIG. 1. Rhombohedral unit cell for antimony.

II. WAVE FUNCTIONS FOR ANTIMONY METAL

Assuming a model of nonoverlapping ions, the field gradient at a point 0 inside the metal is given by[6]

$$q=e\sum_i \zeta_i \frac{3\cos^2\theta_i-1}{r_i^3}-\int \rho(\mathbf{r})\frac{3\cos^2\theta-1}{r^3}d\tau, \quad (1)$$

where $\zeta_i e$ is the charge on an ion core at a point described by the radius vector $\mathbf{r}_i$ with respect to 0 and $-\rho(\mathbf{r})$ is the charge density at a point located at $\mathbf{r}$, due to the conduction electrons. In terms of the wave functions for the conduction electrons, $\rho(\mathbf{r})$ is given by

$$\rho(\mathbf{r})=2e\int |\psi_k(\mathbf{r})|^2 d\tau_k, \quad (2)$$

where $\psi_k(\mathbf{r})$ is the wave function for a conduction electron with wave vector k and the integration extends over the entire volume within the Fermi surface. Equation (1) gives the only parameter q necessary to describe the field gradient in an axially symmetric environment. In the general case, one deals with the second-rank tensor q_{ij}. This tensor has five independent components since it is symmetric, $q_{ij}=q_{ji}$, and has vanishing trace, $\sum_i q_{ii}=0$ (the potential satisfies the Laplace equation at the nuclear site). If we transform to the principal axis system, the tensor becomes diagonal and only q_{xx}, q_{yy}, and q_{zz} do not vanish. Of these three components, only two are independent since $\sum_i q_{ii}=0$. Except for

[14] J. Callaway, in *Solid State Physics*, edited by F. Seitz and D. Turnbull (Academic Press Inc., New York, 1958), Vol. 7, p. 99; W. Kohn, Phys. Rev. **96**, 590 (1954); T. Kjeldaas and W. Kohn, *ibid.* **101**, 66 (1956).

[15] M. H. Cohen, D. A. Goodings, and V. Heine, Proc. Phys. Soc. (London) **73**, 811 (1959); G. D. Gaspari, Wei-Mei Shyu, and T. P. Das, Phys. Rev. **134**, A852 (1964).

[16] A. M. Clogston, A. C. Gossard, V. Jaccarino, and Y. Yafet, Rev. Mod. Phys. **36**, 170 (1964); T. J. Rowland and F. Borsa, Phys. Rev. **134**, A743 (1964); D. O. Van Ostenburg, D. J. Lani, H. D. Trapp, D. W. Procht, and T. J. Rowland, *ibid.* **135**, A455 (1964); R. Kubo and Y. Obata, J. Phys. Soc. Japan **11**, 547 (1956).

[17] G. Wannier and U. N. Upadhaya, Phys. Rev. **136**, A803 (1964); W. Kohn, *ibid.* **115**, 809 (1959); T. P. Das and E. H. Sondheimer, Phil. Mag. **5**, 529 (1960); J. E. Hebborn and E. H. Sondheimer, J. Phys. Chem. Solids **13**, 105 (1960); M. J. Stephen, Proc. Phys. Soc. (London) **79**, 787 (1962); J. E. Hebborn, *ibid.* **80**, 1237 (1962).

[18] R. R. Hewitt and B. F. Williams, Phys. Rev. **129**, 1188 (1963).

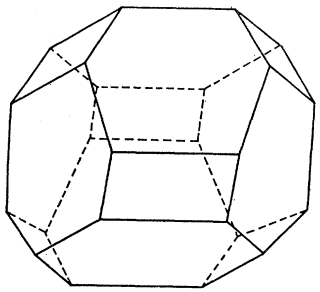

FIG. 2. First Brillouin zone of antimony.

the case of axial symmetry where $q_{xx}=q_{yy}$, we require, in addition to $q_{zz}=q$, an asymmetry parameter η, where

$$\eta=(q_{xx}-q_{yy})/q. \tag{3}$$

Evidently, the calculation of q_{elec}, the electronic contribution to q, and for that matter of $\rho(\mathbf{r})$, requires a knowledge of $\psi_k(\mathbf{r})$ for the entire momentum space within the Fermi surface. Before considering the calculation of $\psi_k(\mathbf{r})$, it is well to review the crystal structure and the available information concerning the Fermi surface of antimony. As shown in Fig. 1, antimony has[19] a rhombohedral unit cell with two ions per unit cell with $a_0=4.4928$ Å and $a=57°12'$ at liquid-nitrogen temperature, and with two ions per unit cell at sites u, u, u and $1-u$, $1-u$, $1-u$, where $u=0.23364$ in units of a_0. If the origin is taken at one of the ions, then the other ion lies on the body diagonal, a little off the body center. Thus, there is axial symmetry about each ion site but no inversion symmetry. Because of the axial symmetry, the field-gradient tensor at the ionic sites does not have any asymmetry parameter and is described entirely by the single quantity q. The ionic contribution to q has a ready been estimated by Taylor and Hygh[20] and found to be too small by about a factor of five compared to experiment. It will be considered further in Sec. III.

The reciprocal lattice is also rhombohedral and is described by the reciprocal basis set ($\mathbf{b}_1$, $\mathbf{b}_2$, and $\mathbf{b}_3$) where

$$\begin{aligned}\mathbf{b}_1&=(\mathbf{a}_2\times\mathbf{a}_3)/\mathbf{a}_1\cdot\mathbf{a}_2\times\mathbf{a}_3,\\ \mathbf{b}_2&=(\mathbf{a}_3\times\mathbf{a}_1)/\mathbf{a}_1\cdot\mathbf{a}_2\times\mathbf{a}_3,\\ \mathbf{b}_3&=(\mathbf{a}_1\times\mathbf{a}_2)/\mathbf{a}_1\cdot\mathbf{a}_2\times\mathbf{a}_3,\end{aligned} \tag{4}$$

and where $\mathbf{a}_1$, $\mathbf{a}_2$, and $\mathbf{a}_3$ are along the edges of the rhombohedron shown in Fig. 1 and are of magnitude a_0.

The first Brillouin zone is indicated in Fig. 2. Since antimony has five electrons per atom and there are two atoms per unit cell in the extended zone picture, the volume within the Fermi surface would be equal to that within the fifth Brillouin zone. In the reduced-zone picture one would expect to have five occupied bands each filling up a volume equal to that of the first zone. In the free-electron limit, the Fermi surface would be expected to be spherical, while in the extreme tight-binding limit one would expect the Fermi surface to approximate closely the boundary of the first Brillouin zone.

Following the most recent work[21] on antimony, the Fermi surface appears to consist of six partial electron ellipsoids and two partial hole ellipsoids located on the fifth-Brillouin-zone boundaries as shown in the reduced zone scheme in Fig. 3 or in the extended zone scheme in Fig. 4. These half-ellipsoids become three complete electron ellipsoids and one complete hole ellipsoid when a particular set of halves are translated by a vector of the reciprocal lattice to their counterparts on an opposite face. In most of the work[21] on the Fermi surface, use has been made of the set of coordinates shown in Fig. 2 to define the equations of these ellipsoids which is different from the choice of axis we have made use of in the field-gradient calculation.

The equation of the principal electron ellipsoid (the one shown in Fig. 3, the others not being shown) having the correct symmetry is

$$E_F=(\hbar^2/2m_0)(\alpha_{11}k_{x'}{}^2+\alpha_{22}k_{y'}{}^2+\alpha_{33}k_{z'}{}^2+2\alpha_{23}k_{y'}k_{z'}). \tag{5}$$

However, if we describe the ellipsoid using its own principal axes as co-ordinates, we have

$$E_F=(\hbar^2/2m_0)(\alpha_1k_x{}^2+\alpha_2k_y{}^2+\alpha_3k_z{}^2). \tag{6}$$

The equations for the other two nonprincipal ellipsoids are obtained by a rotation of the coordinates by $+120°$ and $-120°$ about the z axis used to define Eq. (5). The hole ellipsoid is given in its principal axis system by an equation similar to (6) but with semi-axes defined by β_1, β_2 and β_3 instead of α_1, α_2 and α_3. The volumes of the ellipsoids are very small, compared to the rest of the occupied regions of the Brillouin zone, of the order of about 10^{-5} electrons per atom.

In summary, it appears then that for a property such as the charge density that involves the entire occupied momentum space, one could approximate the Fermi

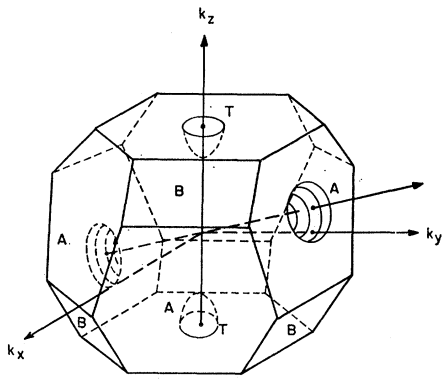

FIG. 3. Electron and hole ellipsoids in reduced zone picture.

[19] W. B. Pearson, *Lattice Spacings and Structure of Metals* (Pergamon Press, Inc., New York, 1958), p. 24; C. S. Barrett, Australian J. Phys. **13**, 209 (1963); C. S. Barrett, P. Cucka, and K. Haefner, Acta Cryst. **16**, 651 (1963).

[20] T. T. Taylor and E. H. Hygh, Phys. Rev. **129**, 1193 (1963).

[21] J. Ketterson and Y. Eckstein, Phys. Rev. **132**, 1885 (1963) and earlier references quoted there.

surface by the Brillouin-zone boundary and subsequently correct for the small pockets of holes and electrons.[22] This is the assumption we shall make in the field-gradient calculation as it leads to a very important simplification which will now be discussed.

In terms of the Wannier functions $a_n(\mathbf{r}-\mathbf{M})$, the Bloch functions for the conduction electrons may be written as

$$\psi_n(\mathbf{k},\mathbf{r})=N^{-1/2}\sum_{\mathbf{M}} e^{+i\mathbf{k}\cdot\mathbf{M}}a_n(\mathbf{r}-\mathbf{M}), \qquad (7)$$

where the suffix n refers to a particular band. From Eq. (2), the electron density $\rho(\mathbf{r})$ is therefore given by

$$\rho(\mathbf{r})=e\sum_n \int d^3k\,|\psi_n(\mathbf{k},\mathbf{r})|^2$$

$$=\frac{e}{N}\sum_n\sum_{\mathbf{M},\mathbf{M}'}\int e^{i\mathbf{k}\cdot(\mathbf{M}'-\mathbf{M})}a_n^*(\mathbf{r}-\mathbf{M})a_n(\mathbf{r}-\mathbf{M}')d^3k$$

$$=e\textstyle\sum_n\sum_{\mathbf{M}}|a_n(\mathbf{r}-\mathbf{M})|^2, \qquad (8)$$

where we have made use of the fact that the integration in $\mathbf{k}$ extends over the first Brillouin zone and hence

$$\int e^{i\mathbf{k}\cdot(\mathbf{M}'-\mathbf{M})}d^3k=N\delta_{\mathbf{M}',\mathbf{M}}. \qquad (9)$$

The integration over k in Eq. (2) is therefore obviated and instead we have the problem of determining the Wannier function. Before describing the choice we made for the Wannier functions, it will be helpful to consider some properties of the Wannier function.

Using Eq. (5), one can obtain the one-electron equation satisfied by the Wannier-functions. Thus, if $\mathcal{H}_e$ represents the one-electron Hamiltonian, then, using the definition of Wannier functions,

$$a_n(\mathbf{r}-\mathbf{M})=N^{-1/2}\textstyle\sum_{\mathbf{k}} e^{-i\mathbf{k}\cdot\mathbf{M}}\psi_n(\mathbf{k},\mathbf{r}),$$

we get

$$\mathcal{H}_e a_n(\mathbf{r}-\mathbf{M})=N^{-1/2}\textstyle\sum_{\mathbf{k}} e^{-i\mathbf{k}\cdot\mathbf{M}}\epsilon_n(\mathbf{k})\psi_n(\mathbf{k},\mathbf{r}), \qquad (10)$$

where $\epsilon_n(\mathbf{k})$ is the one-electron eigenvalue for the Bloch function $\psi_n(\mathbf{k},\mathbf{r})$, that is

$$\mathcal{H}_e\psi_n(\mathbf{k},\mathbf{r})=\epsilon_n(\mathbf{k})\psi_n(\mathbf{k},\mathbf{r}). \qquad (11)$$

Making a Fourier analysis of $\epsilon_n(\mathbf{k})$ in real space, namely,

$$\epsilon_n(\mathbf{k})=N^{-1/2}\textstyle\sum_{\mathbf{M}} E_n(\mathbf{M})e^{i\mathbf{k}\cdot\mathbf{M}}, \qquad (12)$$

and

$$E_n(\mathbf{M})=N^{-1/2}\textstyle\sum_{\mathbf{k}} e^{-i\mathbf{k}\cdot\mathbf{M}}\epsilon_n(\mathbf{k}),$$

Eq. (10) reduces to

$$\mathcal{H}_e a_n(\mathbf{r}-\mathbf{M})=\textstyle\sum_{\mathbf{M}'} E_n(\mathbf{M}')a_n(\mathbf{r}-\mathbf{M}-\mathbf{M}'). \qquad (13)$$

Hence $a_n(\mathbf{r}-\mathbf{M})$ is not an exact eigenfunction of the one-electron Hamiltonian. From Eq. (13), we get

$$E_n(0)=\int a_n^*(\mathbf{r})\mathcal{H}_e a_n(\mathbf{r})d\tau \qquad (14)$$

and

$$E_n(\mathbf{M})=\int a_n^*(\mathbf{r}-\mathbf{M})\mathcal{H}_e a_n(\mathbf{r})d\tau. \qquad (15)$$

For a tight-binding approximation, it follows from (14) and (15) that $E_n(\mathbf{M})\ll E_n(0)$. This means that in Eq. (12) for $\epsilon_n(\mathbf{k})$, only the first term on the right-hand side is the most significant. Thus, minimizing the energy $\epsilon_n(\mathbf{k})$ is almost equivalent to minimizing $E_n(0)$ as given by (14). In addition, for the extreme tight-binding limit, $\mathcal{H}_e$ reduces to the atomic one-electron Hamiltonian and Eq. (13) reduces to the one-electron Schrödinger equation for the free-atomic state.

These two considerations enable us to make a reasonable choice for the Wannier functions for the five fully occupied bands of antimony. First, we notice that the orthogonalized atomic orbitals (OAO) introduced by Löwdin[23] reduce to free-atomic orbitals for large distances of separation between atoms or for the extreme tight-binding limit when the overlaps of atomic orbitals on neighboring orbitals becomes negligible. Second, we have considered OAO on different centers which are orthogonal to each other where $i=s$, p_x, p_y and p_z acts as the band index n. Both these properties are shared by Wannier functions. This makes our OAO good candidates to use for the Wannier functions $a_n(\mathbf{r}-\mathbf{M})$. In general, we have to combine a set of OAO of requisite symmetry to get the symmetric Wannier function as shown in Appendix A. As a first approximation, one can use as the Wannier functions the OAO corresponding to the outermost valence states of the atoms. Thus, using Eq. (8) we get

$$\rho(\mathbf{r})=-e\textstyle\sum_i(1+\delta_{is})[\sum_{\mathbf{A}}|\psi_i(\mathbf{r}-\mathbf{A})|^2 +\sum_{\mathbf{B}}|\psi_i(\mathbf{r}-\mathbf{B})|^2], \qquad (16)$$

where $\psi_i(\mathbf{r}-\mathbf{A})$ and $\psi_i(\mathbf{r}-\mathbf{B})$ are orthogonalized atomic orbitals centered on A and B, respectively. For a more

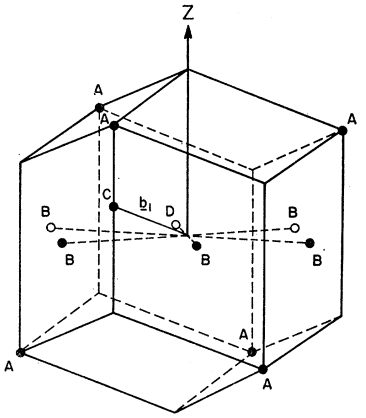

FIG. 4. Electron and hole ellipsoids in extended zone picture. The points B are the positions of the electron ellipsoids and points A are the positions of the hole ellipsoids. The point C is the center of the reduced zone shown in Fig. 3.

[22] An estimate of the contribution to the field gradient from pockets of holes and electrons has been carried out [E. H. Hygh, Ph.D. thesis, University of California, Riverside, 1964 (unpublished)]. It was found to affect the result in only the fourth significant figure.

[23] P. O. Löwdin, J. Chem. Phys. **19**, 1396, 1570, 1678 (1951).

comprehensive discussion concerning the derivation of Eqs. (16) and (22) for $\rho(\mathbf{r})$ see Appendix A. Thus, keeping terms only up to second order in the overlap between orbitals on nearest neighbors, the ψ_i are given by

$$\psi_i(\mathbf{r}-\mathbf{M})=\phi_i(\mathbf{r}-\mathbf{M})-\tfrac{1}{2}\sum_j\sum_{\mathbf{N}}S_{ij}(\mathbf{M},\mathbf{N})\phi_j(\mathbf{r}-\mathbf{N})+\tfrac{3}{8}\sum_j\sum_l\sum_{\mathbf{N}}\sum_{\mathbf{L}}S_{il}(\mathbf{M},\mathbf{N})S_{lj}(\mathbf{N},\mathbf{L})\phi_j(\mathbf{r}-\mathbf{L}), \quad (17)$$

where

$$S_{ij}(\mathbf{M},\mathbf{N})=\int\phi_i^*(\mathbf{r}-\mathbf{M})\phi_j(\mathbf{r}-\mathbf{N})d\tau \quad (18)$$

and the ϕ_i are the atomic orbitals of the free atom. In Eq. (17), if $\mathbf{M}$ refers to an A type ion, then the summation over $\mathbf{N}$ refers to only the nearest-neighbor B ions and $\mathbf{L}$ refers to the original A ion, as well as the A-type nearest neighbors of the B ions. The neglect of direct overlaps between A-type ions can be justified from a consideration of the amplitudes of the (A,B) and (A,A) overlaps presented in Sec. III.

As a second approximation, one can consider the mixing between the OAO ψ_i produced by the noncentral terms in the one-electron Hamiltonian $\mathcal{H}_e$. Thus, since the antimony atoms in the lattice are not at centers of symmetry, we shall have odd-order spherical harmonic terms in the potential in addition to the even-order terms of nonzero order. Of these terms only the Y_1^0 term can cause any admixture between the OAO that we have considered; and therefore, correct to first-order terms we can write the crystal Hamiltonian in atomic units (Rydbergs) as

$$\mathcal{H}_e=+\sum_{\mathbf{M}}\{-\nabla^2+V_0(|\mathbf{r}-\mathbf{M}|)+C_1^0(|\mathbf{r}-\mathbf{M}|)Y_1^0(\theta_M,\phi_M)\}. \quad (19)$$

Assuming that the OAO ψ_i are obtained by minimizing $E_n(0)$ as given by (14) without the C_1^0 term in (19), we derive the following expressions for the perturbed Wannier functions which minimize the value of $E_n(0)$ in (14) arising from the entire $\mathcal{H}_e$ in (19):

$$\begin{aligned}a_s(\mathbf{r}-\mathbf{A})&=(1/\sqrt{2})\{(2-\lambda^2)^{1/2}\psi_s(\mathbf{r}-\mathbf{A})-\lambda\psi_z(\mathbf{r}-\mathbf{A})\},\\ a_z(\mathbf{r}-\mathbf{A})&=(1/\sqrt{2})\{(2-\lambda^2)^{1/2}\psi_z(\mathbf{r}-\mathbf{A})+\lambda\psi_s(\mathbf{r}-\mathbf{A})\},\\ a_{x,y}(\mathbf{r}-\mathbf{A})&=\psi_{x,y}(\mathbf{r}-\mathbf{A}),\end{aligned} \quad (20)$$

and corresponding expressions for $a_i(\mathbf{r}-\mathbf{B})$ with $\mathbf{A}$ replaced by $\mathbf{B}$ and with the signs in the a_s and a_z functions changed. This sign change is due to the fact that the crystal Hamiltonian suffers a change in sign in the $C_1^0(|\mathbf{r}-\mathbf{M}|)Y_1^0(\theta_m,\varphi_m)$ term when expanded about a $\mathbf{B}$ lattice site. In Eqs. (20),

$$\begin{aligned}&\lambda=(1-1/(1+2n^2))^{1/2}\approx 0, \quad \text{for} \quad n\approx 0,\\ &n=\beta/(W_s-W_z),\\ &\beta=\int\psi_z^*(\mathbf{r})C_1^0(r)rY_1^0(\theta,\phi)\psi_s(\mathbf{r})d^3\mathbf{r},\\ &W_i=\int\psi_i^*(\mathbf{r})(-\nabla^2+V_0(\mathbf{r}))\psi_i(\mathbf{r})d^3\mathbf{r}.\end{aligned} \quad (21)$$

These equations are correct to order λ^2 and also to second order in the overlap between A and B ions only. In higher order there would be additional mixing between orbitals on A and B sites. The mixing of the s and p OAO on each site is somewhat analogous to the concept of s-p hybridization in the simple chemical picture proposed recently by Cohen, Falicov, and Golin.[24] From Eq. (16), using equations (20) and corresponding equations for $a_i(\mathbf{r}-\mathbf{B})$, we get the following expression for $\rho(r)$, namely;

$$\rho(\mathbf{r})=e[|\psi_x(\mathbf{r})|^2+|\psi_y(\mathbf{r})|^2+|\psi_z(\mathbf{r})|^2+2|\psi_s(\mathbf{r})|^2+\sum_{\mathbf{B}}\{|\psi_x(\mathbf{r}-\mathbf{B})|^2+|\psi_y(\mathbf{r}-\mathbf{B})|^2+|\psi_z(\mathbf{r}-\mathbf{B})|^2+2|\psi_s(\mathbf{r}-\mathbf{B})|^2\}+\lambda\{-|\psi_s^*(\mathbf{r})\psi_z(\mathbf{r})|+\sum_{\mathbf{B}}|\psi_s^*(\mathbf{r}-\mathbf{B})\psi_z(\mathbf{r}-\mathbf{B})|\}] \quad (22)$$

keeping only those terms up to first order in the perturbation. In Eq. (22), the summation over the B ions extends over all the six nearest neighbors of the A ion which is taken as the origin. It is assumed that to the order of approximation considered [to second order in overlap in $S_{ij}(\mathbf{A},\mathbf{B})$], the other A ions, besides the one at the origin, contribute negligibly to the density in the vicinity of the central ion.

III. CALCULATION OF THE FIELD GRADIENT AND COMPARISON WITH EXPERIMENT

To calculate q due to the electrons, we have to compute the second term on the right-hand side of Eq. (1) using the expression for $\rho(\mathbf{r})$ given by (22). However, since we have several different orientations of the lines joining A and the several B neighbors, it is convenient to simplify the expression for $\rho(\mathbf{r})$ as given by (22), with the help of the orthogonality conditions for the orbitals and crystal symmetry considerations. The various terms $|\psi_i(\mathbf{r}-\mathbf{M})|^2$ may be rewritten in terms of the atomic orbitals $\Phi_i(\mathbf{r}-\mathbf{M})$ as follows:

$$|\psi_i(\mathbf{r})|^2=|\phi_i(\mathbf{r})|^2-\tfrac{1}{2}\sum_{j,\mathbf{B}}S_{ij}(\mathbf{A},\mathbf{B})\{\phi_j^*(\mathbf{r}-\mathbf{B})\phi_i(\mathbf{r})+\phi_j(\mathbf{r}-\mathbf{B})\phi_i^*(\mathbf{r})\}+\tfrac{1}{4}\sum_{j,\mathbf{B}}\sum_{j',\mathbf{B}'}S_{ij}(\mathbf{A},\mathbf{B})S_{ij'}(\mathbf{A},\mathbf{B}')\{\phi_{j'}^*(\mathbf{r}-\mathbf{B}')\phi_j(\mathbf{r}-\mathbf{B})\}+\tfrac{3}{4}\sum_{j,\mathbf{B}}\sum_{m,\mathbf{A}'}S_{im}(\mathbf{A},\mathbf{B})S_{mj}(\mathbf{B},\mathbf{A}')\{\phi_j^*(\mathbf{r}-\mathbf{A}')\phi_i(\mathbf{r})+\phi_j(\mathbf{r}-\mathbf{A}')\phi_i^*(\mathbf{r})\}, \quad (23)$$

[24] M. H. Cohen, L. M. Falicov, and S. Golin, IBM J. Res. Develop. 8, 215 (1964).

$$|\psi_i(\mathbf{r}-\mathbf{B})|^2=|\phi_i(\mathbf{r}-\mathbf{B})|^2-\tfrac{1}{2}\sum_{j\mathbf{A}''}S_{ij}(\mathbf{B},\mathbf{A}'')\{\phi_j^*(\mathbf{r}-\mathbf{A}'')\phi_i(\mathbf{r}-\mathbf{B})+\phi_j(\mathbf{r}-\mathbf{A}'')\phi_i^*(\mathbf{r}-\mathbf{B})\}$$
$$+\tfrac{1}{4}\sum_{j\mathbf{A}''}\sum_{j'\mathbf{A}'''}S_{ij}(\mathbf{B},\mathbf{A}'')S_{ij'}(\mathbf{B},\mathbf{A}''')\phi_j^*(\mathbf{r}-\mathbf{A}'')\phi_{j'}(\mathbf{r}-\mathbf{A}''')$$
$$+\tfrac{3}{4}\sum_{j\mathbf{A}''}\sum_{m\mathbf{B}''}S_{im}(\mathbf{B},\mathbf{A}'')S_{mj}(\mathbf{A},\mathbf{B}'')\{\phi_j^*(\mathbf{r}-\mathbf{B}'')\phi_i(\mathbf{r}-\mathbf{B})+\phi_j(\mathbf{r}-\mathbf{B}'')\phi_i^*(\mathbf{r}-\mathbf{B})\}. \quad (24)$$

We can simplify Eqs. (23) and (24) by noting that only the terms involving wave functions on A and its nearest-neighbor B ions would effectively contribute to the field gradient at the A nucleus. The other terms will be too distant to contribute to q through the short-ranged operator $(3\cos^2\theta_A-1)/r_A^3$ in (1). Thus, in the summations in (23) and (24), we have to take $A'=A''=A'''=A$ and $B'=B''=B''=\{\mathrm{NN}\}_A$, where $\{\mathrm{NN}\}$ means "nearest neighbor of." Further, since the orbitals on the atoms are s and p orbitals, one can show from the orthonormal properties of spherical harmonics that, as far as terms on atom A are concerned, only product terms in the density involving two p orbitals of the same symmetry (x, y, or z) will contribute to the field-gradient integral. In addition, from symmetry considerations, of the various terms in $\rho(\mathbf{r})$ involving products of two different orbitals on a B atom alone, only those involving s and p_z orbitals can contribute to the field gradient at the A nucleus. Combining all these simplications, we can rewrite Eqs. (23) and (24) for $|\psi_i(\mathbf{r})|^2$ and $|\psi(\mathbf{r}-\mathbf{B})|^2$ in somewhat simpler forms:

$$|\psi_i(\mathbf{r})|^2=[1+\tfrac{3}{4}\sum_{m\mathbf{B}}S_{im}^2(\mathbf{A},\mathbf{B})]|\phi_i(\mathbf{r})|^2-\tfrac{1}{2}\sum_{j,\mathbf{B}}S_{ij}(\mathbf{A},\mathbf{B})\{\phi_j^*(\mathbf{r}-\mathbf{B})\phi_i(\mathbf{r})+\phi_j(\mathbf{r}-\mathbf{B})\phi_i^*(\mathbf{r})\}$$
$$+\tfrac{1}{4}\sum_{j,\mathbf{B}}S_{ij}^2(\mathbf{A},\mathbf{B})|\phi_j(\mathbf{r}-\mathbf{B})|^2+\tfrac{1}{4}\sum_{\mathbf{B}}S_{is}(\mathbf{A},\mathbf{B})S_{iz}(\mathbf{A},\mathbf{B})\{\phi_s^*(\mathbf{r}-\mathbf{B})\phi_z(\mathbf{r}-\mathbf{B})+\phi_s(\mathbf{r}-\mathbf{B})\phi_z^*(\mathbf{r}-\mathbf{B})\}, \quad (25)$$

$$|\psi_i(\mathbf{r}-\mathbf{B})|^2=[1+\tfrac{3}{4}\textstyle\sum_m S_{mi}^2(\mathbf{A},\mathbf{B})]|\phi_i(\mathbf{r}-\mathbf{B})|^2$$
$$-\tfrac{1}{2}\textstyle\sum_j S_{ji}(\mathbf{A},\mathbf{B})\{\phi_i^*(\mathbf{r}-\mathbf{B})\phi_j(\mathbf{r})+\phi_i(\mathbf{r}-\mathbf{B})\phi_j^*(\mathbf{r})\}+\tfrac{1}{4}\textstyle\sum_j S_{ji}^2(\mathbf{A},\mathbf{B})|\phi_j(\mathbf{r})|^2$$
$$+\tfrac{3}{4}\textstyle\sum_j\sum_m S_{mi}(\mathbf{A},\mathbf{B})S_{mj}(\mathbf{A},\mathbf{B})\{\phi_i^*(\mathbf{r}-\mathbf{B})\phi_j(\mathbf{r}-\mathbf{B})+\phi_i(\mathbf{r}-\mathbf{B})\phi_j^*(\mathbf{r}-\mathbf{B})\}(\delta_{is}\delta_{jz}+\delta_{iz}\delta_{js}), \quad (26)$$

where the Kronecker delta, δ_{is} in (26), for example, is zero when i is not an s orbital and $\delta_{is}=1$ when i is an s orbital. In a similar manner, the terms in $\rho(\mathbf{r})$ which contribute to the field gradient through the λ term may be written as

$$\psi_s^*(\mathbf{r})\psi_z(\mathbf{r})=\tfrac{3}{8}\sum_{j\mathbf{B}}S_{sj}(\mathbf{A},\mathbf{B})S_{zj}(\mathbf{A},\mathbf{B})|\phi_z(\mathbf{r})|^2+\tfrac{1}{4}\sum_{j\mathbf{B}}S_{sj}(\mathbf{A},\mathbf{B})S_{zj}(\mathbf{A},\mathbf{B})|\phi_j(\mathbf{r}-\mathbf{B})|^2$$
$$+\tfrac{1}{4}\textstyle\sum_{\mathbf{B}}S_{ss}(\mathbf{A},\mathbf{B})S_{zz}(\mathbf{A},\mathbf{B})\phi_z^*(\mathbf{r}-\mathbf{B})\phi_s(\mathbf{r}-\mathbf{B})+\tfrac{1}{4}\textstyle\sum_{\mathbf{B}}S_{sz}(\mathbf{A},\mathbf{B})S_{zs}(\mathbf{A},\mathbf{B})\phi_z(\mathbf{r}-\mathbf{B})\phi_s^*(\mathbf{r}-\mathbf{B})$$
$$-\tfrac{1}{2}\sum_{j\mathbf{B}}S_{sj}(\mathbf{A},\mathbf{B})\phi_j^*(\mathbf{r}-\mathbf{B})\phi_z(\mathbf{r})-\tfrac{1}{2}\sum_{j\mathbf{B}}S_{zj}(\mathbf{A},\mathbf{B})\phi_j(\mathbf{r}-\mathbf{B})\phi_s^*(\mathbf{r}), \quad (27)$$

$$\psi_s^*(\mathbf{r}-\mathbf{B})\psi_z(\mathbf{r}-\mathbf{B})=[1+\tfrac{3}{4}\textstyle\sum_m S_{ms}(\mathbf{A},\mathbf{B})S_{mz}(\mathbf{A},\mathbf{B})]\phi_s^*(\mathbf{r}-\mathbf{B})\phi_z(\mathbf{r}-\mathbf{B})$$
$$+\tfrac{3}{8}\textstyle\sum_m S_{ms}(\mathbf{A},\mathbf{B})S_{mz}(\mathbf{A},\mathbf{B})\{|\phi_s(\mathbf{r}-\mathbf{B})|^2+|\phi_z(\mathbf{r}-\mathbf{B})|^2\}+\tfrac{1}{4}\textstyle\sum_i S_{is}(\mathbf{A},\mathbf{B})S_{iz}(\mathbf{A},\mathbf{B})|\phi_i(\mathbf{r})|^2$$
$$-\tfrac{1}{2}\textstyle\sum_i S_{is}(\mathbf{A},\mathbf{B})\phi_i^*(\mathbf{r})\phi_z(\mathbf{r}-\mathbf{B})-\tfrac{1}{2}\textstyle\sum_i S_{iz}(\mathbf{A},\mathbf{B})\phi_i^*(\mathbf{r})\phi_s(\mathbf{r}-\mathbf{B}). \quad (28)$$

On substituting Eqs. (25), (26), (27), and (28) in Eq. (22) for the charge density $\rho(\mathbf{r})$, the charge density $\rho(\mathbf{r})$ can be rearranged in three parts: one part $\rho_v^{AA}(\mathbf{r})$ involving products of orbitals on atom A above, a second part $\rho_v^{AB}(\mathbf{r})$ involving products of orbitals, one of which is on A and the other on a neighboring B atom, and finally a part $\rho_v^{BB}(\mathbf{r})$ containing products of orbitals on B atoms only:

$$\rho_v^{AA}(\mathbf{r})=e\sum_{\substack{i=x,\\y,z}}[1+\sum_{\mathbf{B}}\sum_{\substack{m=s,\\x,y,z}}S_{im}^2(\mathbf{A},\mathbf{B})+\tfrac{1}{4}\sum_{\mathbf{B}}S_{is}^2(\mathbf{A},\mathbf{B})]|\phi_i(\mathbf{r})|^2$$
$$-\lambda(3e/8)[\sum_{\mathbf{B}}\sum_{\substack{m=s,\\x,y,z}}S_{sm}(\mathbf{A},\mathbf{B})S_{zm}(\mathbf{A},\mathbf{B})]|\phi_z(\mathbf{r})|^2+\tfrac{1}{4}\lambda e\sum_{\substack{i=x,\\y,z}}[\sum_{\mathbf{B}}S_{is}(\mathbf{A},\mathbf{B})S_{iz}(\mathbf{A},\mathbf{B})]|\phi_i(\mathbf{r})|^2, \quad (29)$$

$$\rho_v^{AB}(\mathbf{r})=-\tfrac{1}{2}e\sum_{\substack{i=s,\\x,y,z}}(1+\delta_{is})\sum_{\mathbf{B}}\sum_{\substack{j=s,\\x,y,z}}S_{ij}(\mathbf{A},\mathbf{B})\{\phi_j^*(\mathbf{r}-\mathbf{B})\phi_i(\mathbf{r})+\phi_j(\mathbf{r}-\mathbf{B})\phi_i^*(\mathbf{r})\}$$
$$-\tfrac{1}{2}e\sum_{\substack{i=s,\\x,y,z}}(1+\delta_{is})\sum_{\mathbf{B}}\sum_{\substack{j=s,\\x,y,z}}S_{ij}(\mathbf{A},\mathbf{B})\{\phi_i^*(\mathbf{r}-\mathbf{B})\phi_j(\mathbf{r})+\phi_i(\mathbf{r}-\mathbf{B})\phi_j^*(\mathbf{r})\}$$
$$+\lambda\tfrac{1}{2}e[\sum_{\mathbf{B}}\sum_{\substack{j=s,\\x,y,z}}S_{sj}(\mathbf{A},\mathbf{B})\phi_j^*(\mathbf{r}-\mathbf{B})\phi_z(\mathbf{r})+\sum_{\mathbf{B}}\sum_{\substack{j=s,\\x,y,z}}S_{zj}(\mathbf{A},\mathbf{B})\phi_j(\mathbf{r}-\mathbf{B})\phi_s^*(\mathbf{r})]$$
$$-\lambda\tfrac{1}{2}e[\sum_{\mathbf{B}}\sum_{\substack{i=s,\\x,y,z}}S_{is}(\mathbf{A},\mathbf{B})\phi_i^*(\mathbf{r})\phi_z(\mathbf{r}-\mathbf{B})+\sum_{\mathbf{B}}\sum_{\substack{i=s,\\x,y,z}}S_{iz}(\mathbf{A},\mathbf{B})\phi_i^*(\mathbf{r})\phi_s(\mathbf{r}-\mathbf{B})],\quad(30)$$

$$\rho_v^{BB}(\mathbf{r})=e\sum_{\substack{i=s,\\x,y,z}}(1+\delta_{is})\sum_{\mathbf{B}}[1+\tfrac{3}{4}\sum_{\substack{m=s,\\x,y,z}}S_{mi}^2(\mathbf{A},\mathbf{B})]|\phi_i(\mathbf{r}-\mathbf{B})|^2+\tfrac{1}{4}e\sum_{\substack{i=s,\\x,y,z}}(1+\delta_{is})\sum_{\mathbf{B}}[\sum_{\substack{j=s,\\x,y,z}}S_{ij}^2(\mathbf{A},\mathbf{B})|\phi_j(\mathbf{r}-\mathbf{B})|^2]$$
$$+\tfrac{1}{4}e\sum_{\substack{i=s,\\x,y,z}}(1+\delta_{is})\sum_{\mathbf{B}}S_{is}(\mathbf{A},\mathbf{B})S_{iz}(\mathbf{A},\mathbf{B})[\phi_s^*(\mathbf{r}-\mathbf{B})\phi_z(\mathbf{r}-\mathbf{B})+\phi_s(\mathbf{r}-\mathbf{B})\phi_z^*(\mathbf{r}-\mathbf{B})]$$
$$+\tfrac{3}{4}e\sum_{\substack{i=s,\\x,y,z}}(1+\delta_{is})\sum_{\mathbf{B}}\sum_{\substack{j=s,\\x,y,z}}\sum_{\substack{m=s,\\x,y,z}}S_{mi}(\mathbf{A},\mathbf{B})S_{mj}(\mathbf{A},\mathbf{B})[\phi_i^*(\mathbf{r}-\mathbf{B})\phi_j(\mathbf{r}-\mathbf{B})+\phi_i(\mathbf{r}-\mathbf{B})\phi_j^*(\mathbf{r}-\mathbf{B})](\delta_{is}\delta_{jz}+\delta_{iz}\delta_{js})$$
$$-\lambda\tfrac{1}{4}e\sum_{\mathbf{B}}\sum_{\substack{j=s,\\x,y,z}}S_{sj}(\mathbf{A},\mathbf{B})S_{zj}(\mathbf{A},\mathbf{B})|\phi_j(\mathbf{r}-\mathbf{B})|^2-\lambda\tfrac{1}{4}e\sum_{\mathbf{B}}S_{ss}(\mathbf{A},\mathbf{B})S_{zz}(\mathbf{A},\mathbf{B})\phi_s(\mathbf{r}-\mathbf{B})\phi_z^*(\mathbf{r}-\mathbf{B})$$
$$-\lambda\tfrac{1}{4}e\sum_{\mathbf{B}}S_{sz}(\mathbf{A},\mathbf{B})S_{zs}(\mathbf{A},\mathbf{B})\phi_s^*(\mathbf{r}-\mathbf{B})\phi_z(\mathbf{r}-\mathbf{B})+\lambda e\sum_{\mathbf{B}}[1+\tfrac{3}{4}\sum_{\substack{m=s,\\x,y,z}}S_{ms}(\mathbf{A},\mathbf{B})S_{mz}(\mathbf{A},\mathbf{B})]\phi_s^*(\mathbf{r}-\mathbf{B})\phi_z(\mathbf{r}-\mathbf{B})$$
$$+\lambda\tfrac{3}{8}e\sum_{\mathbf{B}}\sum_{\substack{m=s,\\x,y,z}}S_{ms}(\mathbf{A},\mathbf{B})S_{mz}(\mathbf{A},\mathbf{B})[|\phi_s(\mathbf{r}-\mathbf{B})|^2+|\phi_z(\mathbf{r}-\mathbf{B})|^2].\quad(31)$$

In calculating the field gradient using the expressions for the charge-density terms ρ_v^{AA}, ρ_v^{AB}, and ρ_v^{BB}, we next have to consider the evaluation of a number of two-center integrals. Typical of these two-center integrals are the following:

$$S_{ij}(\mathbf{A},\mathbf{B})=\int\phi_i^*(\mathbf{r})\phi_j(\mathbf{r}-\mathbf{B})d\tau,$$
$$q_{ij}^{\mathbf{AB}}=\left(\frac{16\pi}{5}\right)^{1/2}\int\phi_i^*(\mathbf{r})\frac{1}{r^3}Y_2^0(\theta,\phi)\phi_j(\mathbf{r}-\mathbf{B})d\tau,\quad(32)$$
$$q_{ij}^{\mathbf{BB}}=\left(\frac{16\pi}{5}\right)^{1/2}\int|\phi_i(\mathbf{r}-\mathbf{B})|^2\frac{Y_2^0(\theta,\phi)}{r^3}d\tau.$$

The procedure that we employed to evaluate such integrals is one formulated by Löwdin and often termed as the α-function technique in the literature. Thus, if the choice of coordinate axes and polar coordinates about two centers B and A is taken as in Fig. 5, then a wave function centered about center B can be expanded around center A as follows:

$$(f_{NL}(\mathrm{R})/R)Y_L^M(\Theta,\Phi)=\sum_{l=0}^{\infty}(K_{LM}/K_{lM})\alpha_l(NLM|B,r)Y_l^M(\theta,\phi),\quad(33)$$

where B is the distance between the centers A and B and

$$K_{LM}=\left(\frac{2L+1}{4\pi}\frac{(L-|M|)!}{(L+|M|)!}\right)^{1/2}.\quad(34)$$

The α function, $\alpha_l(NLM|B,r)$, is defined by

$$\alpha_l(NLM|B,r)=\frac{2\pi K_{lM}^2}{Br}\int_{|B-r|}^{|B+r|}f_{NL}(R)\times P_L^{|M|}(\cos\Theta)P_l^{|M|}(\cos\theta)dR,\quad(35)$$

where $\cos\Theta$ and $\cos\theta$ in (35) are expressed in terms of r and R by the equations

$$\cos\theta=(B^2+r^2-R^2)/2BR,\qquad\cos\Theta=(B^2+R^2-r^2)/2Br.\quad(36)$$

However, the X, Y, and Z axes are chosen for the field-gradient operator and the p_x, p_y, and p_z orbitals on the A and B type atoms are determined by the crystal symmetry, as shown in Fig. 1. These axes are different from the axes in Fig. 5 which are convenient to use for two-center integrals. One therefore has to make use of the rules for transformation of spherical harmonics from one coordinate to another. The pertinent coefficients D_{iM}^L, for the transformations involved in the present context, are discussed in Appendix B. Thus we can express some of the quantities involved in the integrals (32) in the following convenient forms more suitable

for performing the two-center integrals:

$$\phi_i(\mathbf{r})=(f_{51}(r)/r)\sum_{M=-1}^{1} D_{iM}{}^{1}Y_1{}^{M}(\theta,\phi),$$

$i=s$, p_x, p_y, and p_z. The quantities $D_{iM}{}^{1}$ are derived in the Appendix and represent functions of the Eulerian angles θ_R, Φ_R and ψ_R which relate the crystal coordinate system with a local system for which the line AB joining a B neighbor to an A atom is taken as the z axis. For the s orbital, which is isotropic, we do not need any transformation relation. Putting it in a different way, $D_{sM}{}^{L}=\delta_{L0}\delta_{M0}$ and so one can write in general

$$\phi_i(\mathbf{r})=(f_{5L'}(r)/r)\sum_{M'=-L'}^{L'} D_{iM'}{}^{L'}Y_{L'}{}^{M'}(\theta,\phi), \quad (37)$$

for $i=s$, p_x, p_y, and p_z. Similarly one can express the operator $q^{\mathrm{op}}=(3\cos^2\theta-1)/r^3$ in (1) defined in the crystal co-ordinate system in terms of the local system as follows:

$$q^{\mathrm{op}}=(16\pi/5)^{1/2}r^{-3}\sum_{M=-2}^{+2} D_{0M}{}^{2}Y_2{}^{M}(\theta,\phi), \quad (38)$$

where the quantities $D_{0M}{}^{2}$ are also derived in Appendix B. In the integrals (32) we used both orbitals centered on A and B sites. For expressing the latter in terms of the local polar co-ordinates θ, ϕ at A, one has first to apply a transformation as in (37) and then use the Eq.

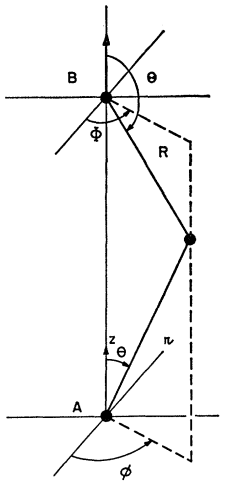

FIG. 5. Choice of coordinates for two-center integrals.

(33) for the α-function expansion. Combining the two processes, we have

$$\phi_j(\mathbf{r}-\mathbf{B})=\sum_{M=-L}^{L}\sum_{l=0}^{\infty}(K_{LM}/K_{lM})\times D_{jM}{}^{L}\alpha_l(5LM\,|\,Br)Y_l{}^{M}(\theta,\phi). \quad (39)$$

The overlap integral $S_{ij}(AB)$ in (32) can then be expressed in the following form by combining Eqs. (37) and (39):

$$S_{ij}(\mathbf{AB})=\sum_{M=-L'}^{L'} D_{jM}{}^{L}D_{iM}{}^{L'*}\int_0^{\infty}\alpha_{L'}(5LM\,|\,B,r)f_{5L'}(r)r\,dr. \quad (40)$$

In a similar manner the integral $q_{ij}{}^{AB}$ can also be expressed in terms of a number of radial integrals involving α functions:

$$q_{ij}{}^{\mathbf{AB}}=2\sum_{M'=-L'}^{L'}\sum_{m=-2}^{+2}\sum_{M=-L}^{L}\sum_{l=|2-L'|}^{L'+2} D_{iM'}{}^{L'}D_{0m}{}^{2}D_{jM}{}^{L*}\times\left(\frac{2L'+1}{2l+1}\right)^{1/2}\begin{pmatrix}2 & L' & l\\ 0 & 0 & 0\end{pmatrix}\begin{pmatrix}2 & L' & l\\ m & M' & m+M'\end{pmatrix}\cdot\delta_{M,m+M'}\frac{K_{LM}}{K_{lM}}\int\frac{f_{5L'}(r)}{r^2}\alpha_l(5LM\,|\,B,r)dr. \quad (41)$$

The Clebsch-Gordan coefficients appear in making use of products of spherical harmonics, namely in the relation

$$Y_{L'}{}^{M'}Y_{L''}{}^{M''}=\sum_{L=|L'-L''|}^{L'+L''}\left(\frac{(2L'+1)(2L''+1)}{4\pi(2L+1)}\right)^{1/2}\begin{pmatrix}L' & L'' & L\\ 0 & 0 & 0\end{pmatrix}\begin{pmatrix}L' & L'' & L\\ M' & M'' & M'+M''\end{pmatrix}Y_L{}^{M'+M''}. \quad (42)$$

For evaluating the integrals in $q_{ij}{}^{BB}$, we have to expand integrals like $\Phi_i(r-B)\Phi_j(r-B)$ in terms of α functions and spherical harmonics about the center A. One then obtains, using Eqs. (32), (38), and (39)

$$q_{ij}{}^{\mathbf{BB}}=\sum_{l'=0}^{2L}\sum_{M_1=-L}^{L}\sum_{M_2=-L}^{L} D_{iM_1}{}^{L}D_{jM_2}{}^{L*}\frac{2L+1}{(4\pi(2l'+1))^{1/2}}\begin{pmatrix}L & L & l'\\ 0 & 0 & 0\end{pmatrix}\begin{pmatrix}L & L & l'\\ -M_1 & M_2 & M_2-M_1\end{pmatrix}\times\frac{K_{l',M_2-M_1}}{K_{2,M_2-M_1}}\delta_{0,M_2-M_1}\left(\frac{16\pi}{5}\right)^{1/2}\int_0^{\infty}\frac{\alpha_2(5l'M_2-M_1\,|\,B,r)}{r}dr. \quad (43)$$

When i is an s orbital and j a p_z orbital about B, we obtain, by a similar procedure, the following expression for

$q_{sp_z}{}^{BB}$:

$$q_{sp_z}{}^{BB}=D_{z0}{}^{1}\frac{1}{(4\pi)^{1/2}}\frac{K_{10}}{K_{20}}\left(\frac{16\pi}{5}\right)^{1/2}\int_0^\infty\frac{\alpha_2(51M\,|\,B,r)}{r}dr. \tag{44}$$

In Eqs. (43) and (44) above, the α functions are given by Eqs. (45) and (46), respectively:

$$\alpha_2(5l'M_2-M_1\,|\,B,r)=2\pi K_{2,M_2-M_1}{}^2\int_0^\pi\left(\frac{f_{5l'}(R)}{R}\right)^2 P_{l'}{}^{|M_2-M_1|}(\cos\Theta)P_2{}^{|M_2-M_1|}(\cos\theta)\sin\theta\,d\theta, \tag{45}$$

$$\alpha_2(51M\,|\,B,r)=2\pi K_{2,M}{}^2\int_0^\pi\frac{f_{50}f_{51}(R)}{R^2}P_1{}^{|M|}(\cos\Theta)P_2{}^{|M|}(\cos\theta)\sin\theta\,d\theta. \tag{46}$$

In Table I are tabulated the integrals[25] involving α functions, namely,

$$C_{NLM}{}^{N'L'}=\int_0^\infty\alpha_{L'}(NLM\,|\,B,r)f_{N'L'}(r)r\,dr, \tag{47}$$

that are required to obtain the necessary $S_{ij}(AB)$ between orbitals A and those on the nearest three and next-nearest three neighbors of A. It is seen that because of the somewhat larger distance to the next-nearest neighbors ($0.74446a_R$, where a_R is the rhombohedral lattice constant) as compared to the nearest-neighbor distance ($0.64532a_R$), the integrals $C_{NLM}{}^{N'L}$ for the next-nearest neighbors are smaller. By the same token, the two center integrals involving orbitals on third-nearest ($0.95790a_R$) and more distant neighbors would be expected to be much smaller. This expectation is also supported by Table II where the values of $f_{50}(R)$ and $f_{50}(R)/R$ are tabulated at the position of A when the $5s$ orbital is at different neighboring sites. These considerations justify our neglect of overlap and two center integrals for ions beyond the nearest three and next-nearest three neighbors of A.

In Table III are tabulated the overlap integrals $S_{ij}{}^{AB}$ between orbitals on the atom A and those on the three nearest and next-nearest neighbors. Again the overlaps are in general smaller when j refers to next-nearest neighbors of A instead of the nearest except in special cases, when geometrical factors exemplified by the quantities $D_{iM}{}^{L'}$ tend to reverse the order. In Table IV we have tabulated the α-function integrals which occur in the evaluation of $q_{ij}{}^{AB}$ and $q_{ij}{}^{BB}$ in Eqs. (41) and (43). The same remarks apply for the observed variation of these integrals with distances to the neighbors of A, as were made for the overlap integrals.

In Table V are tabulated the values of the various contributors to the field gradient q, namely q_{ionic}, the field gradient produced by the point charges $+5e$ on the Sb^{+5} ion, $q_e{}^{AA}$, $q_e{}^{AB}$, $q_e{}^{BB}$, the electronic contributors to the field gradient of the local, nonlocal and distant types, respectively, $q_e{}^{\text{total}}$ the total electronic contribution, q^{total} the total calculated field gradient including the ionic and electronic contributions and finally q^{expt}, the experimental value. The results in the second column represent the contributions from the various calculated terms without including antishielding (or shielding) effects[26] due to the polarization of core electron states by the nuclear quadrupole moment. The results in the third column include correction factors due to antishielding effects. Since the charge distributions that produce the various contributions to the field gradient in Table V are disposed differently with respect to the core electrons of the antimony atom A under study, the different contributions q_{ionic}, $q_e{}^{AA}$, $q_e{}^{AB}$, and $q_e{}^{BB}$ will all in general be subject to different antishielding correction factors. This can be understood by an analysis of the expression for the antishielding factor.

TABLE I. Table of two-center integrals required to calculate overlap integrals.

Integral	Nearest neighbors	Next-nearest neighbors
$C_{500}{}^{50}$	0.12675	0.06968
$C_{510}{}^{50}$	0.15712	0.10555
$C_{500}{}^{51}$	−0.47137	−0.31644
$C_{510}{}^{51}$	−0.31394	−0.26153
$C_{511}{}^{51}$	0.16255	0.10248

TABLE II. Values of $f_{50}(R)$ and $f_{50}(R)/R$ at A for $5s$ orbitals at different sites.

R[a]	$f_{50}(R)$	$\frac{f_{50}(R)}{R}$
0.00000	0.000000	1.63904
0.64532	0.064390	0.01174
0.74446	0.030705	0.00484
0.95790	0.005846	0.00072
1.00000	0.003962	0.00046
1.16790	0.001089	0.00011

[a] Distance to the neighbors given in units of the rhombohedral lattice parameter $a_R=4.5066$ Å.

[25] The Sb atomic wave functions used are those of F. Herman and S. Skillman, *Atomic Structure Calculations* (Prentice-Hall, Inc., Englewood Cliffs, New Jersey, 1963).

[26] R. M. Sternheimer, Phys. Rev. **80**, 102 (1950); **84**, 244 (1951); **86**, 316 (1952); **95**, 736 (1954); R. M. Sternheimer and H. M. Foley, *ibid.* **102**, 731 (1956); T. P. Das and R. Bersohn, *ibid.* **102**, 733 (1956).

TABLE III. Values of the overlap integrals S_{ij}^{AB} for orbitals on various B sites.

Neighbor	1	2	3	4	5	6
ss	0.06968	0.06958	0.06968	0.12675	0.12675	0.12675
sx	0.14932	−0.07461	−0.07461	−0.23279	0.11639	0.11639
sy	0.00000	0.12922	−0.12922	0.00000	0.20158	−0.20158
sz	−0.10562	−0.10562	−0.10562	0.14098	0.14098	0.14098
xs	−0.14923	0.07461	0.07461	0.23279	−0.11639	−0.11639
xx	−0.14003	0.04185	0.04185	−0.18605	0.07540	0.07540
xy	0.00000	0.10501	−0.10501	0.00000	−0.15095	0.15095
xz	0.17165	−0.08583	−0.08583	0.21115	−0.10558	−0.19558
yz	0.00000	−0.12922	0.12922	0.00000	−0.20158	0.20158
yx	0.00000	0.10501	0.10501	0.00000	−0.15095	0.15095
yy	0.10248	−0.07940	−0.07940	0.16255	−0.09890	−0.09890
yz	0.00000	0.14866	−0.14866	0.00000	−0.18286	0.18286
zs	0.10562	0.10562	0.10562	−0.14098	−0.14098	−0.14098
zx	0.17165	−0.08583	−0.08583	0.21115	−0.10588	−0.10588
zy	0.00000	0.14866	−0.14866	0.00000	−0.18286	0.18286
zz	−0.01902	−0.01902	−0.01902	0.03466	0.03466	0.03466

Thus, let us assume that the nuclear quadrupole moment induces a net quadrupole moment density $Q_i(r')$ at a point r' in the core-electron system. If we have a point charge at a position r relative to the nucleus, the field gradient at the nucleus ($q=\partial^2V/\partial z^2$) due to the point charge will be altered to

$$q'=q(1-\gamma(r)),$$

where

$$\gamma(r)=\frac{1}{Q}\left[\int_0^r Q_i(r')dr'+r^5\int_r^\infty Q_i(r')r'^{-5}dr'\right]. \quad (48)$$

Now, if instead of an external point charge, we have a charge density $\rho(\mathbf{r})$, then the effective antishielding factor will be given by

$$\gamma=\langle\gamma(r)\rangle=\frac{\int_0^\infty \gamma(r)\rho(\mathbf{r})[(3\cos^2\theta-1)/r^3]d\tau}{\int_0^\infty \rho(\mathbf{r})[(3\cos^2\theta-1)/r^3]d\tau}. \quad (49)$$

For the local atomic term q_{AA}, the antishielding factor will thus be given by

$$\gamma_{AA}=\langle\gamma(r)\rangle_{AA}=\frac{\int_0^\infty \gamma(r)|\phi_z(\mathbf{r})|^2[(3\cos^2\theta-1)/r^3]d\tau}{\int_0^\infty |\phi_z(\mathbf{r})|^2[(3\cos^2\theta-1)/r^3]d\tau}. \quad (50)$$

For the nonlocal field gradient q_{AB}, the relevant antishielding term would be obtained considering the charge density $\phi_i(\mathbf{r})\phi_j^*(\mathbf{r}-\mathbf{B})$

$$\gamma_{AB}=\langle\gamma(r)\rangle_{AB}=\frac{\int_0^\infty \gamma(r)\phi_i(\mathbf{r})\phi_j^*(\mathbf{r}-\mathbf{B})[(3\cos^2\theta-1)/r^3]d\tau}{\int_0^\infty \phi_i(\mathbf{r})\phi_j^*(\mathbf{r}-\mathbf{B})[(3\cos^2\theta-1)/r^3]d\tau}. \quad (51)$$

Correspondingly, the pertinent antishielding factor for the distant term q_{BB} would be γ_{BB} obtained by using the charge density $|\Phi_i(r-B)|^2$ in Eq. (49)

$$\gamma_{BB}=\langle\gamma(\mathbf{r})\rangle_{BB}=\frac{\int_0^\infty \gamma(r)|\phi_i(\mathbf{r}-\mathbf{B})|^2[(3\cos^2\theta-1)/r^3]d\tau}{\int_0^\infty |\phi_i(\mathbf{r}-\mathbf{B})|^2[(3\cos^2\theta-1)/r^3]d\tau}. \quad (52)$$

Since the charge distribution described by $|\Phi_i(\mathbf{r}-\mathbf{B})|^2$ is almost totally external to the charge distribution on the A atom, one would expect γ_{BB} to be reasonably close to the antishielding factor $\gamma_\infty=\gamma(r\to\infty)$ due to an external point charge, which is the pertinent factor to use for the ionic term. To evaluate γ_{AA}, γ_{AB}, γ_{BB}, and γ_∞ would require a calculation of $\gamma(r)$. The quantity γ_{AA} is of importance for the nuclear quadrupole interaction in the atom while γ_∞ is of importance in considering nuclear

TABLE IV. Values of two-center field-gradient integrals (a) AB terms: $S_{NLM}^{anl}=\int_0^\infty \alpha_a(NLM|B,r)f_{nl}(r)(1/r^2)dr$, and (b) BB terms: $R_{NLM}^{all'}=\int_0^\infty \alpha_a(NLM|B,r)(1/r)dr$.

	Integral	Nearest neighbor (4,5,6)	Next-nearest neighbor (1,2,3)
	S_{500}^{2s0}	0.0127383	0.0049778
	S_{510}^{2s0}	0.0166691	0.0067051
	S_{511}^{2s0}	−0.0029381	−0.0014820
	S_{500}^{1s1}	0.0042516	−0.0028520
(a)	S_{510}^{1s1}	0.0298405	0.0017994
	S_{511}^{1s1}	0.0033512	0.0017934
	S_{500}^{3s1}	0.0299980	−0.0008214
	S_{510}^{3s1}	0.0633093	0.0149961
	S_{511}^{3s1}	0.0040966	−0.0945720
	R_{500}^{2ss}	0.0299464	0.0195680
	R_{500}^{2pp}	0.0277733	0.0187957
	R_{520}^{2pp}	0.0083588	0.0045802
(b)	R_{521}^{2pp}	−0.0063260	−0.0033789
	R_{522}^{2pp}	0.0017336	0.0008794
	R_{510}^{2sp}	−0.0121790	−0.0071153
	R_{511}^{2sp}	0.0041872	0.0023956

TABLE V. Table of contributions from various sources to the field gradient at antimony nucleus.

Electric-field gradient term	Principal contribution: Without Sternheimer correction	Principal contribution: With Sternheimer correction	Perturbation contribution: Without Sternheimer correction	Perturbation contribution: With Sternheimer correction	Total contribution with Sternheimer correction and with $\lambda=0.10$
q_{ionic}	16.8×10^{12}	252×10^{12}			252×10^{12}
q_e^{AA}	1617.5×10^{12}	1804×10^{12}	-525.6×10^{12}	-586×10^{12}	1745×10^{12}
q_e^{AB}	8.4×10^{12}	23×10^{12}	-24.3×10^{12}	-66×10^{12}	16×10^{12}
q_e^{BB}	-5.4×10^{12}	-81×10^{12}	-22.0×10^{12}	-330×10^{12}	-114×10^{12}
q_e^{total}	1620.5×10^{12}	1746×10^{12}	-571.9×10^{12}	-982×10^{12}	1648×10^{12}
q^{total}	1637.3×10^{12}	1998×10^{12}			1900×10^{12}
q^{exp} [a]					1889×10^{12}

[a] This is the mean value of data on Sb^{121} and Sb^{123} taken by Hewitt and Williams (Ref. 18) and by Murakawa (Ref. 43).

quadrupole interaction in ionic compounds of antimony. Unfortunately, no results are currently available for either γ_{AA} or γ_∞. We have, therefore, to make estimates of γ_{AA} and γ_∞ from the results of calculation in neighboring atoms and ions. The calculated value[27] of γ_∞ for the isoelectronic ion In^{+3} is -15.33. The antimony ion Sb^{+5} would be expected to have a smaller value for γ_∞ because of its larger effective charge which causes the electronic orbitals to be more tightly bound. Such a behavior is indeed found for other isoelectronic ions where the values of γ_∞ are available. We estimate[28] a value of γ_∞ equal to -14 for Sb^{+5} ion. As we shall see later in this section, the calculated total field gradient does not depend critically on the choice for γ_∞. Since the charge density $|\phi_i(\mathbf{r}-\mathbf{B})|^2$ is almost completely external to the electron orbitals on the A atom, it is a good approximation to use $\gamma_{BB}=\gamma_\infty$.

Sternheimer[26] has calculated values of γ_{AA} for a number of elements. Of particular interest to our present situation are his calculations on the shielding factors for $5p$ and $6p$ (excited) atomic states of cesium. This element is a good reference to use for estimating γ_{AA} for the $5p$ state of antimony because the $5p$ and $6p$ states of cesium lie, respectively, below and above the $5p$ state of antimony. This would indicate that the $5p$ electron in cesium would be more internal than that in antimony. In addition, the core states in cesium atom would be more tightly bound then in antimony and, therefore, lead to smaller $Q_i(r)$ in Eq. (48). Both these considerations lead one to expect that the magnitude of γ_{AA} for the $5p$ state of cesium may be regarded as a lower limit for γ_{AA} for the antimony $5p$ state. The magnitude of γ_{AA} for the $6p$ state of cesium can similarly be regarded as an upper limit for γ_{AA} for the antimony atom, although this estimate is not as clear-cut because the two considerations now lead to opposite conclusions. Thus we expect that

$$0.212<-\gamma_{AA}<0.018.$$

Adopting the arithmetic mean of the two limits, we shall use $(1-\gamma_{AA})=1.115$. Finally, since $\phi_i^*(\mathbf{r}-\mathbf{B})\phi_i(\mathbf{r})$ in Eq. (51) is not as internal as $|\phi_i(\mathbf{r})|^2$ nor as completely external as $|\phi_i(\mathbf{r}-\mathbf{B})|^2$, we made the choice for γ_{AB} as the geometric mean of γ_{AA} and γ_{BB}. This leads to a value of 2.722 for $(1-\gamma_{AB})$.

From Table V, it appears that after applying the relevant Sternheimer antishielding corrections, the contribution q_e^{AA} still exceeds by far all the other contributions. The contribution q_e^{BB} becomes more significant than q_e^{AB} after the antishielding correction has been applied, because of the much larger value of $(1-\gamma_{BB})$ as compared to $(1-\gamma_{AB})$. The total electronic contribution, in the absence of the λ-dependent crystal-field "perturbation" term then comes out as

$$q'_e{}^{\text{total}}=(1804+23-81)\times10^{12}$$
$$=1746\times10^{12}\ \text{esu/cm}^3. \quad (53)$$

This result is almost an order of magnitude larger than the ionic contribution of $q'_{\text{ionic}}=252\times10^{12}$ esu/cm^3 and of the same sign. Combining the ionic and electronic contributions, we have

$$q'^{\text{total}}=1998\times10^{12}\ \text{esu/cm}^3, \quad (54)$$

in good agreement with the experimental value.

The perturbation contribution comes out from Table V as

$$q'_e{}^{\text{pert}}\approx-982\times10^{12}\lambda\ \text{esu/cm}^3. \quad (55)$$

If the crystal-field perturbation produced a potential which leads to a perturbation energy approximately 5% of the atomic p-orbital energy, then we have $n\approx0.05$ in Eq. (21) and $\lambda\approx0.10$. This would then lead from (55) to

$$q'_e{}^{\text{pert}}\approx-98\times10^{12}\ \text{esu/cm}^3. \quad (56)$$

Combining $q'_e{}^{\text{pert}}$ with $q'_e{}^{\text{total}}$ in Eqs. (53) and q'^{total} in Eq. (54) we get

$$q_e{}^{\text{total}}\approx1648\times10^{12}\ \text{esu/cm}^3 \quad (57)$$

[27] E. G. Wikner and G. Burns, Phys. Rev. **121**, 155 (1961).
[28] E. G. Wikner and T. P. Das, Phys. Rev. **109**, (1958).

for the electronic contribution alone, and

$$q^{\text{total}} \approx 1900 \times 10^{12} \text{ esu/cm}^3, \quad (58)$$

in even better agreement with experiment than the result in (54) without the effect of the crystal-field perturbation. While the very close agreement with experiment in both cases is certainly fortuitous in view of all the approximations made, it is certainly fair to say that the electronic contribution to the field gradient has been reasonably well-estimated using the model we have employed. Various sources of error and their total estimated effect on the calculated field gradient will be discussed in Sec. 5.

IV. ISOTROPIC AND ANISOTROPIC KNIGHT SHIFTS

An additional property of the conduction electrons in a metal that one obtains out of nuclear magnetic resonance measurements is the Knight shift[9] δ, namely the fractional shift in the resonance frequency as compared to that for the nucleus in some reference sample. Often the reference sample is an aqueous solution of the ion containing the nucleus under study.

If the metal is cubic, there is only one parameter δ which represents the Knight shift completely. Bloembergen and Rowland[29] have shown that for a noncubic metal, the tensor properties of the Knight shift become more apparent and one has to use two parameters δ_{iso} and δ_{ax} for metals in which the nuclei are at sites of threefold and higher symmetry. For sites of lower symmetry, three parameters, δ_{iso}, δ_{ax}, and δ_{asym} are required for a complete description of the Knight shift tensor. The situation is very much similar to that for the electric field-gradient tensor at a nuclear site.

The Knight shift originates from the magnetic hyperfine interaction between the conduction electrons and the nuclei described by the dipolar and Fermi contact Hamiltonians:

$$\mathcal{H}_{eN}^{\text{dip}} = \tfrac{1}{2}\gamma_e\gamma_N\hbar^2 \sum_{ij}\left\{\frac{\mathbf{I}_i\cdot\mathbf{S}_j}{r_{ij}^3} - \frac{3(\mathbf{I}_i\cdot\mathbf{r}_{ij})(\mathbf{S}_j\cdot\mathbf{r}_{ij})}{r_{ij}^5}\right\}, \quad (59)$$

$$\mathcal{H}_{eN}^{F} = \frac{8\pi}{3}\gamma_e\gamma_N\hbar^2 \sum_{ij}\mathbf{I}_i\cdot\mathbf{S}_j\delta(\mathbf{r}_{ij}), \quad (60)$$

where $\mathbf{I}_i$ and $\mathbf{S}_j$ are the spins of ith nucleus and jth electron, respectively, $\mathbf{r}_{ij}=\mathbf{r}_j-\mathbf{R}_i$ is the radius vector joining the ith nucleus and jth electron and γ_e and γ_N are the magnetogyric ratios of the electron and nucleus, respectively. Alternatively one can describe the hyperfine interaction by means of the magnetic fields H_{eN}^{dip} and H_{eN}^{F} that are produced by the electron j at the position of the nucleus i:

$$\mathbf{H}_{eN}^{\text{dip}} = \tfrac{1}{2}\gamma_e\hbar\textstyle\sum_j(\mathbf{S}_j/r_{ij}^3 - 3\mathbf{r}_{ij}(\mathbf{S}_j\cdot\mathbf{r}_{ij})/r_{ij}^5), \quad (61)$$

$$\mathbf{H}_{eN}^{F} = (8\pi/3)\gamma_e\hbar\textstyle\sum_j\mathbf{S}_j\delta(\mathbf{r}_{ij}). \quad (62)$$

[29] N. Bloembergen and T. J. Rowland, Acta Met. **1**, 731 (1953).

When there is no applied magnetic field there is no net magnetic polarization of the electrons and so no net field is produced by the electron at the nuclear sites. However, when there is a magnetic field present, the number of electrons that are parallel to the field is smaller than that of those that are antiparallel. This spin polarization leads to the important Pauli paramagnetic contribution to the susceptibility of metals. Townes, Herring, and Knight[30] and Bloembergen and Rowland[29] have shown, using Eqs. (61) and (62), that the additional field produced by the conduction electrons at the nucleus is given by

$$H = H_{\text{ext}}\{1+\delta_{\text{iso}}+\delta_{\text{ax}}(3\cos^2\theta_H - 1) + \delta_{\text{asym}}\sin^2\theta_H\cos 2\phi_H\}, \quad (63)$$

where θ_H,ϕ_H represent the polar coordinates of the direction of the applied field H_{ext} with respect to the principal axes of the Knight-shift tensor which is determined by the local symmetry around the nucleus. Expressions for δ_{iso}, δ_{ax}, and δ_{asym} are given by Eqs. (64), (65), and (66) in terms of the wave functions for the conduction electrons:

$$\delta_{\text{iso}} = (8\pi/3\Omega_F)\sum_i\langle|b_i(\mathbf{k};0)|^2\rangle_{EF}\zeta_p, \quad (64)$$

$$\delta_{\text{ax}} = \frac{1}{\Omega_F}\left(\frac{16\pi}{5}\right)^{1/2}\int\sum_i\left[\langle|b_i(\mathbf{k};\mathbf{r})|^2\rangle_{EF}\times\frac{1}{r^3}Y_2^0(\theta,\phi)d^3r\right]\zeta_p, \quad (65)$$

$$\delta_{\text{asym}} = \frac{1}{\Omega_F}\left(\frac{32\pi}{15}\right)^{1/2}\int\sum_i\left[\langle|b_i(\mathbf{k};\mathbf{r})|^2\rangle_{EF}\times\frac{1}{r^3}Y_2^2(\theta,\phi)d^3\mathbf{r}\right]\zeta_p. \quad (66)$$

In Eqs. (64), (65), and (66), Ω_F represents the area of the Fermi surface and ζ_p is the spin susceptibility of the conduction electrons. The sum over i in Eqs. (64), (65), and (66) extends over the entire surface, so that on dividing by Ω_F and summing over i, we get an average over the entire Fermi surface. Since the antimony nuclei are at sites of threefold symmetry, $\delta_{\text{asym}}=0$, and we have only to obtain δ_{iso} and δ_{ax}.

The Pauli paramagnetic susceptibility ζ_p is given formally by

$$\zeta_p = -\mu_0^2\int\frac{\partial f_0}{\partial E}g(E)dE, \quad (67)$$

where $g(E)$ is the density of states per unit energy interval per atom, f_0 is the Fermi function,[31] and μ_0, the Bohr magneton. For low temperatures, Eq. (67) simpli-

[30] C. H. Townes, C. Herring, and W. D. Knight, Phys. Rev. **77**, 852 (1950).

[31] C. Kittel, *Solid State Physics* (John Wiley & Sons, Inc., New York, 1959), 2nd edition, p. 251.

fies to $\zeta_p=\mu_0^2 g(E_F)$. Since in some of the better metals exchange and correlation effects among the conduction electrons have been shown[32] to contribute significantly to ζ_p, we would like to comment briefly on the role of such mechanisms in antimony. An approximate form for ζ_p including correlation and exchange effects is given by

$$\zeta_p=\mu_0^2 g(E_F) \times\left\{1-\frac{\alpha r_s}{\pi}+\tfrac{3}{4}(\alpha r_s)^2[0.225-0.676\ln r_s]\right\}^{-1}, \quad (68)$$

where

$$\alpha=(4/9\pi)^{1/3},$$

and

$$r_s=(9\pi/4)^{1/3}(me^4/2\hbar^2)^{1/2}E_F^{-1/2}.$$

This correction is necessary only if the electrons are nearly free; thus, in the case of most metals, $r_s\gg 1$ and the correction is large. However, since the electrons in antimony are not as free as in the case of most metals, the mass, m is much smaller. For this case, $r_s\approx 1$ and we can essentially take the expression in the brackets to be unity. Available information on the Fermi surface of antimony indicates that it has three identical electron ellipsoids and one hole ellipsoid. For an ellipsoidal surface, the general expression for the density of states per unit energy interval per atom in the crystal space,[33]

$$g(E)=\frac{dN(E)}{dE}=\frac{\Omega}{(2\pi)^3}\int\frac{dS_k}{|\nabla_k E(k)|},$$

reduces to

$$g(E)=\Omega/4\pi^2(\alpha_1\alpha_2\alpha_3)^{-1/2}(2m_0/\hbar^2)^{3/2}E^{1/2}, \quad (69)$$

where the energy surface is given by

$$E(\mathbf{k})=(\hbar^2/2m_0)(\alpha_1 k_x^2+\alpha_2 k_y^2+\alpha_3 k_z^2), \quad (70)$$

and Ω is the atomic volume. The parameters $\alpha_i=m_0/m_i$ are related to the effective masses m_i and, for antimony, they are found to be quite large. Using Eq. (69) for $g(E_F)$ together with Ketterson and Eckstein's values[21] of the effective mass parameters and Shoenberg's value[3] for the Fermi energy ($E_F=18.6\times10^{-14}$ ergs), the spin-susceptibilities are obtained as

$$\begin{aligned}\zeta_p(\text{electrons})&=5.28\times10^{-8}\Omega,\\ \zeta_p(\text{holes})&=2.82\times10^{-8}\Omega,\end{aligned} \quad (71)$$

where Ω is the atomic volume. This evaluation of ζ_p has ignored the effects of the spin-orbit coupling. As discussed by Kubo and Obata,[34] the spin-orbit interaction can be considered approximately to lead to an enhancement of ζ_p by a factor of $(1+\lambda/\Delta)$, where λ is the spin-orbit coupling parameter and Δ is the mean width of the conduction band. In the absence of a reliable knowledge of λ and Δ, it is difficult to estimate this factor quantitatively. However, if one considers the rough picture suggested by Cohen *et al.*,[25] for arsenic, the mean bandwidth of antimony ought to be of the order of 1.2 eV. The average spin-orbit coupling in the free atom is of the order 0.6 eV so that it is reasonable to take one-half as an upper limit for λ/Δ. Thus a susceptibility enhancement factor of about $\frac{3}{2}$ seems a reasonable, upper limit.

The other quantities that we have to calculate in order to obtain the isotropic and axial Knight shift are, from Eqs. (64) and (65), of the form

$$\frac{\delta_{\text{iso}}}{((8\pi/3\Omega_F)\zeta_p)}=\sum_i\langle|b_i(\mathbf{k};0)|^2\rangle_{E_F}, \quad (72)$$

$$\frac{\delta_{\text{ax}}}{((1/\Omega_F)(16\pi/5)^{1/2}\zeta_p)}=\sum_i\int\langle|b_i(\mathbf{k};\mathbf{r})|^2\rangle_{E_F} \times\frac{Y_2^0(\theta,\phi)}{r^3}d^3\mathbf{r}. \quad (73)$$

Since only the s function has finite density at the nucleus ($r=0$), we have only to calculate $\langle|b_s(\mathbf{k};0)|^2\rangle_{E_F}$ for the isotropic Knight shift δ_{iso}. From Eq. (5), the average over the Fermi surface involves

$$\langle|e^{i(\mathbf{k}_0(j)+\Delta\mathbf{k})\cdot\mathbf{M}}|\rangle_{E_F} =e^{i\mathbf{k}_0(j)\cdot\mathbf{M}}\int_{\text{F.S.}}e^{i\Delta\mathbf{k}\cdot\mathbf{M}}\frac{d\mathbf{S}_k}{|\nabla_k E|}\Big/\int_{\text{F.S.}}\frac{d\mathbf{S}_k}{|\nabla_k E|}, \quad (74)$$

where $\mathbf{M}=(\mathbf{A}-\mathbf{A}')$, $(\mathbf{B}-\mathbf{B}')$. The net $\mathbf{k}$ vector in the extended zone picture can be separated into two parts; $\mathbf{k}_0(j)$, which is the vector joining the center of the Brillouin zone to the center of a hole or electron ellipsoid $j=(h,e)$ and $\Delta\mathbf{k}$ which is a vector from the center of the ellipsoid to a point on its surface. The ratio of the two integrals in (74) may be shown to be close to unity[22], since the sizes of the ellipsoids are very small. The vectors $\mathbf{k}_0(j)$, for the three electron ellipsoids and one hole ellipsoid model, are given by

$$\mathbf{k}_0(e)=\tfrac{1}{2}(\mathbf{b}_2-\mathbf{b}_3)\quad(\text{principal}), \quad (75)$$

$$\mathbf{k}_0(e)=\tfrac{1}{2}(\mathbf{b}_1-\mathbf{b}_2)\quad(\text{nonprincipal}), \quad (76)$$

$$\mathbf{k}_0(e)=\tfrac{1}{2}(\mathbf{b}_3-\mathbf{b}_1)\quad(\text{nonprincipal}), \quad (77)$$

and

$$\mathbf{k}_0(h)=\tfrac{3}{2}\mathbf{b}_1+\tfrac{1}{2}\mathbf{b}_2+\tfrac{1}{2}\mathbf{b}_3. \quad (78)$$

The vectors $\mathbf{b}_i$ are the primitive vectors of the reciprocal lattice listed in Sec. II. Using Eqs. (5) and (74), we then get

$$\langle|b_i(\mathbf{k};\mathbf{r})|^2\rangle_{E_F}=\sum_{\mathbf{A}}\sum_{\mathbf{A}'}[\psi_i^*(\mathbf{r}-\mathbf{A}')\psi_i(\mathbf{r}-\mathbf{A}) +\psi_i^*(\mathbf{r}-\mathbf{A}'-\Delta\mathbf{R})\psi_i(\mathbf{r}-\mathbf{A}-\Delta\mathbf{R})]\cdot e^{i\mathbf{k}_0(j)\cdot(\mathbf{A}-\mathbf{A}')}. \quad (79)$$

[32] D. Pines, *Elementary Excitations in Solids* (W. A. Benjamin, Inc., New York, 1963), p. 153.
[33] J. Callaway, *Energy Band Theory* (Academic Press Inc., New York, 1964), p. 37.
[34] R. Kubo and Y. Obata, Ref. 16.

TABLE VI. Contributions to the isotropic and anisotropic Knight shifts from electron and hole Fermi surfaces.

Component parts of Fermi surface	Isotropic Knight shift δ_{ax} Without spin-orbit interaction	Isotropic Knight shift δ_{ax} With spin-orbit interaction	Anisotropic Knight shift δ_{ax} (contribution due to p_x, p_y, and p_z bands) Without spin-orbit interaction	Anisotropic Knight shift δ_{ax} (contribution due to p_x, p_y bands) With spin-orbit interaction	Anisotropic Knight shift δ_{ax} (contribution due to p_x, p_y band) Without spin-orbit interaction	Anisotropic Knight shift δ_{ax} (contribution due to p_x, p_y band) With spin-orbit interaction
Electron ellipsoid contribution	3.157×10^{-4}	4.736×10^{-4}	-0.101×10^{-4}	-0.152×10^{-4}	-2.334×10^{-4}	-3.501×10^{-4}
Hole ellipsoid contribution	1.583×10^{-4}	2.375×10^{-4}	-0.032×10^{-4}	-0.048×10^{-4}	-1.061×10^{-4}	-1.592×10^{-4}
Total theoretical contribution	4.740×10^{-4}	7.111×10^{-4}	-0.133×10^{-4}	-0.200×10^{-4}	-3.395×10^{-4}	-5.093×10^{-4}

From Table IV and our experience with the field-gradient terms in Sec. III, it appears that when we are interested in the Knight shift of the nucleus at the point $A(\mathbf{r}=\mathbf{A}=0)$ we need to consider only the contributions from orbitals $\phi_i(\mathbf{r}-\mathbf{A})$ on the nucleus at A. With this observation in mind, we then get from the wave functions in (17)

$$\psi_s(0)\approx[1+\tfrac{3}{8}\sum_{j,\mathbf{B}} S_{sj}^2(\mathbf{A},\mathbf{B})]\phi_s(0);\quad \mathbf{A}=0,$$

$$\psi_s(\mathbf{A}+\Delta\mathbf{R})\approx-\tfrac{1}{2}S_{ss}(\mathbf{A},\mathbf{B})\phi_s(0);\quad \mathbf{A}+\Delta\mathbf{R}=\mathbf{B}=\{\mathrm{NN}\}_{\mathbf{A}=0} \tag{80}$$

for the s states, and

$$\psi_i(\mathbf{r})\approx[1+\tfrac{3}{8}\sum_{j\mathbf{B}} S_{ij}^2(\mathbf{A},\mathbf{B})]\phi_i(\mathbf{r});\quad \mathbf{A}=0,$$

$$\psi_i(\mathbf{r}-\mathbf{A}-\Delta\mathbf{R})\approx-\tfrac{1}{2}\sum_{j=x,y,z} S_{ji}(\mathbf{A},\mathbf{B})\phi_j(\mathbf{r});\quad \mathbf{A}+\Delta\mathbf{R}=\mathbf{B}=\{\mathrm{NN}\}_{\mathbf{A}=0} \tag{81}$$

for the p states.

Now, in computing the isotropic Knight shift, we can make use of Eqs. (79) and (80) in Eq. (72) for δ_{iso} only if we assume that the s band contributes to all parts of the electron and hole Fermi surfaces. This is admittedly an extreme approximation. It leads to the contributions from the electron and hole surfaces and from the combined effect of both, the amounts shown in the second column of Table VI. Results in the third column of Table VI are obtained on applying an enhancement factor of $\frac{3}{2}$, due to spin-orbit effects mentioned earlier in this section.

To get the axial Knight shift δ_{ax}, we substitute the wave functions (81) in Eq. (79) for $\langle|b_i(\mathbf{k},\mathbf{r})|^2\rangle_{E_F}$ which we then use in Eq. (73) for δ_{ax}. If we now assume that the three bands p_x, p_y, and p_z contribute to the electron and hole Fermi surfaces, then we get the contribution to δ_{ax} shown in the fourth and fifth column of Table VI, respectively, with and without the spin-orbit enhancement factor of $\frac{3}{2}$. In the sixth and seventh columns of Table VI, we have tabulated the values of δ_{ax} one obtains assuming that only the p_x and p_y bands contribute to the Fermi surface both with and without the spin-orbit enhancement factor.

Unfortunately, there are no experimental values currently available for the isotropic and anisotropic Knight shifts in antimony. When experimental values do become available in the future, one can utilize our calculated values of the direct contributions to the isotropic and anisotropic shifts to assess the relative importance of other sources that contribute to the Knight shift. In Sec. V we shall speculate on the possible importance of some of these other contributions to the Knight shift.

V. DISCUSSION

We shall first consider the various sources of error in the calculation of the field gradient and the implications of our results.

The Wannier functions that we have used were not obtained from calculated Bloch functions for the crystal, nor were they obtained by actually carrying out a variational procedure for the crystal.[35] However, the result that the calculated field gradient agrees so well with the observed value, indicates that our use of OAO for the Wannier functions does lead to a charge density that is in over-all agreement with the actual density in the crystal. To be completely rigorous, we should have used a complete set, that is, a linear combination of atomic orbitals for higher excited states of the atom including the continuum as well as the atomic wave function for the state that has been already employed. The neglect of these excited and continuum states may lead us to expect that our choice of Wannier functions yields a more localized state than the actual one. However, when we expand the atomic orbitals of the B center about the A center, we do in fact get an admixture of other states besides the atomic valence. ($5s$, $5px$, $5py$, or $5p_z$) states including the continuum as we desire.

Secondly, the atomic wave functions that were used to obtain the Wannier functions are somewhat inaccurate because they were calculated using the Slater free-electron expression for the exchange potential in the atom. The wave functions calculated in this manner

[35] A variation procedure for localized functions in crystals has been developed by G. F. Koster, Phys. Rev. **89**, 67 (1953); see also J. C. Slater, *ibid.* **87**, 802 (1952).

tend to overemphasize the density in the external regions of the atom and underemphasize the density in the neighborhood of the nucleus. This trend has two conflicting effects on the calculated result. The first effect is to enhance the expectation value used in calculating q_e^{AA}. The second effect is a reduction in the values of the overlap integrals. It is difficult therefore to conclude definitely whether the use of Herman and Skillman's wave functions[25] has enhanced or reduced the calculated field gradient.

Also of importance is the neglect of relativistic effects. These effects are very important in determining the shape and size of the Fermi surface. For example, the spin-orbit coupling in atomic bismuth is large and, consequently, is more than likely of importance in removing the large electron and hole surfaces which might otherwise be predicted by a calculation of the energy bands.[36] In antimony and arsenic, the spin-orbit coupling is not quite as strong. The values of the spin-orbit coupling constants[37] are approximately 0.3, 0.6, and 1.8 eV, respectively, for arsenic, antimony, and bismuth. This means that the spin-orbit interaction energy is of the order of 10% of Herman and Skillman's energy eigenvalue for the $5p$ state of atomic antimony. Although it is necessary to consider spin-orbit effects for energy-band calculations, it is not as important in the field-gradient calculations because we have made use of the experimentally known Fermi surface, and do not have to determine it by calculation. Spin-orbit effects could still affect the calculated value of the field gradient through their effect on the wave functions. However, since the first-order correction in the wave function due to spin-orbit effects involves the ratio of the spin-orbit coupling parameter to the atomic orbital energy, the maximum error in the calculated field gradient due to neglect of spin-orbit effect would not be expected to be more than 10%. A better estimate of the error due to neglect of relativistic effects would require explicit consideration of all relativistic effects on the wave functions in the metal. These include the Darwin term, the mass-velocity energy correction, as well as the spin-orbit coupling. Preliminary attempts to analyze these effects, at least on the energy, have been made by Herman *et al.*,[38] Pratt,[39] and Johnson, Conklin, and Pratt.[40]

Another source of uncertainty is the choice made for the antishielding factor pertinent to the local, nonlocal and distant electronic terms in the expression for the field gradient and also to the ionic contribution. The most important choice is that for the antishielding factor $\langle\gamma(r)\rangle_{AA}$ associated with the local term because this term is the major contributor to the field gradient. The range of uncertainty in $\langle\gamma(r)\rangle_{BB}$, which is nearly equal to γ_∞, is larger than in $\langle\gamma(r)\rangle_{AA}$. However, since the total contribution to the field gradient from the distant electronic and ionic terms is an order of magnitude smaller than that from the local electronic terms, the uncertainty in $\langle\gamma(r)\rangle_{BB}$ has much less effect. In addition, the ionic contribution to the field gradient is actually less significant than Table V would seem to indicate. This fact stems from our neglect of the electronic contribution to the field gradient at nucleus A from Wannier functions centered around atoms more distant than the B neighbors. These functions shield the ionic cores effectively whereas the uniform density ρ_0 considered in the calculation of the ionic term does not. The choice of $B_0{}^0=+5e$ for the charge on the ion cores is therefore an overestimate.

The over-all error in the field gradient due to all the above causes can be estimated roughly as follows. There is probably a $\pm5\%$ error due to the neglect of orthogonalization effects involving distant orbitals and the truncation of the complete set used for expanding the Wannier function beyond the four atomic orbitals ($5s$, $5p_x$, $5p_y$, and $5p_z$) that we have considered in Sec. III. The errors due to inaccuracies in the atomic orbitals used probably cancel each other as we have discussed earlier in this section. Neglect of relativistic effects might introduce as much as $\pm10\%$ error. There is perhaps an error of about $\pm5\%$ in the combined effect of the uncertainty due to the choice of the antishielding factors and the shielding of the charges on the ions by the undulatory charge distribution arising from the conduction electrons. The net error in our calculated field gradient is therefore about $\pm20\%$. The "experimental" value of the field gradient in Table V is based on a knowledge of the quadrupole moments of Sb^{121} (and Sb^{123}) nucleus which is obtained from optical hyperfine data.[41] Since there may easily be an error of 20% in quadrupole moments determined from optical data, the error of $\pm20\%$ in our calculated field gradient is about the same as the uncertainty in the experimental value of the field gradient. The agreement between the theoretical and experimental values of the field gradient is therefore satisfactory to within experimental error.

We have calculated only the direct contribution to the isotropic and anisotropic Knight shifts in Sec. IV. There are a number of other sources which could contribute to both the isotropic and anisotropic Knight shifts. Among these other sources are the core-polarization effect,[15] the Landau diamagnetic contribution[42] and the Van Vleck-Ramsey orbital contribution[16] to the paramagnetic shielding of the nucleus. The influence of the core-polarization effect on the isotropic Knight shift has been analyzed quantitatively in three light metals.[15] In all these metals, the core polarization

[36] M. H. Cohen, L. M. Falicov, and S. Golin, Ref. 25.
[37] E. U. Condon and G. H. Shortley, *The Theory of Atomic Spectra* (Cambridge University Press, London, 1959), p. 275.
[38] F. Herman, C. D. Duglar, F. Cuff, and R. L. Kortum, Phys. Rev. Letters **11**, 541 (1963).
[39] G. W. Pratt, Jr., Phys. Rev. **118**, 462 (1960).
[40] L. E. Johnson, J. B. Conklin, and G. W. Pratt, Jr., Phys. Rev. Letters **11**, 538 (1963).
[41] J. Murakawa, Phys. Rev. **93**, 1232 (1954); **100**, 1369 (1959).
[42] T. P. Das and E. H. Sondheimer, Ref. 17.

has been shown to play a minor role, leading to contributions less than 15% of the pertinent direct contact contributions to the Knight shift. The results in lithium indicate that the s and p parts of the conduction-electron wave functions lead to nearly equal and opposite core-polarization contributions. On the other hand, the results in aluminum metal suggest that one cannot make any definitive conclusions as to the sign of the core-polarization effects due to the s and non-s parts of the conduction electron wave function, since the sign depends also on the core state whose exchange polarization is being studied.

For thallium and thallium alloys, recent workers[16] have suggested that a semiquantitative estimate of the Van Vleck–Ramsey-type contribution indicates that one does not have to invoke direct and core-polarization contributions to the nuclear magnetic shielding constant to explain observed Knight-shift data. On the other hand, the fact that the Knight shift for platinum metal[43] is observed to be negative indicates that core-polarization effects may be significant. It seems to us that, while in some cases there may be a near cancellation of contributions to the Knight shift from different inner shells and different angular parts of the conduction electrons, it is difficult to make any surmises about the importance of the core-polarization contribution without actual quantitative calculations and that its sign could be either positive or negative. Regarding the Landau diamagnetic contribution,[42] it arises from the delocalized plane-wave nature of the conduction electrons which leads to broad conduction bands. We do not think that the Landau term is of any importance in antimony since antimony is a semimetal with very few conduction electrons and also because we can get good agreement with the experimental field gradient using localized OAO wave functions. Finally, we have the Van Vleck–Ramsey-type orbital contribution to consider. The importance of this orbital-type contribution for metals has been emphasized by a number of recent investigators.[16] This contribution requires a departure of the charge density around the nucleus from spherical symmetry and in contrast to the direct and core-polarization contributions, it arises from all electrons and not just those near the Fermi surface. Departures from spherical symmetry that lead to a reorganization of the charge density in the alkali halides due to charge transfer between alkali and halogen ions (termed "covalent binding" in chemical language), has been considered quantitatively by Yosida and Moriya.[44] The effect or reorganization due to overlap of electron orbitals on neighboring ions has been considered by Kondo and Yamashita.[45] The latter authors used OAO wave functions similar to the ones used in our calculation in Sec. III for the field gradient. Since the overlap integrals in antimony metal are considerably larger than in the alkali halides,[46] it seems probable that the orbital-type contributions in antimony metal may be of the same order of magnitude as the experimentally observed Knight shift. It should be remarked that to get a contribution to the anisotropic shift from the orbital-type term, one also requires a departure from cubic symmetry. Anisotropic shielding effects are therefore not seen in alkali halides, but in the case of antimony metal where we have only axial symmetry, we should obtain an orbital-type contribution to the anisotropic Knight shift.

The question of the relative importance of various contributors to the Knight shift, can be settled by careful detailed calculations for both the direct and other contributions. However, such calculations are laborious and have been postponed until experimental data on the isotropic and anisotropic Knight shifts become available. We would like to remark however that one can also obtain qualitative information concerning the relative importance of various contributions to the Knight shift from the study of temperature and pressure dependences of the Knight shift. Thus, since the orbital contribution depends directly on the overlap of the orbitals on neighboring atoms, it would be expected to be sensitively dependent on pressure and temperature.

VI. CONCLUSION

It has been demonstrated that one can take advantage of the semimetallic nature of antimony metal to calculate the electronic contribution to the field gradient in antimony metal. We have shown from a first principle calculation that the conduction electrons can in fact explain the bulk of the observed field gradient, a conclusion that had been previously arrived at by default from a consideration of the ionic contributions only.[11] A parallel calculation in bismuth metal would be of great interest and is currently under progress. For metals which do not involve a volume in k space equal to an integral number of Brillouin zones, the simplifications employed in Secs. II and III cannot be used and an actual calculation of the Bloch or Wannier functions would be required.

The situation concerning the Knight shift is less clear; both the lack of experimental data and a number of other causes that could contribute besides the direct one considered in Sec. IV are specific reasons for this. The direct contribution itself can at best be obtained rather approximately due to lack of detailed knowledge of the wave functions near the Fermi surface. It is hoped that the deliberations in this paper will stimulate additional experimental and theoretical work on the Knight shifts in antimony in particular, and in the semi-

[43] T. J. Rowland, J. Phys. Chem. Solids **7**, 95 (1965); R. E. Walstedt, M. W. Dowley, E. L. Hahn, and C. Froidevaux, Phys. Rev. Letters **8**, 406 (1962).

[44] K. Yosida and T. Moriya, J. Phys. Soc. Japan **11**, 33 (1956).

[45] J. Kondo and J. Yamashita, J. Phys. Chem. Solids **10**, 245 (1959).

[46] D. Ikenberry and T. P. Das, Phys. Rev. **138**, A822 (1965).

metals and their alloys in general. It would be particularly interesting to find out if the anisotropic Knight shift is in fact as small as the direct contribution predicts.

ACKNOWLEDGMENTS

The authors are grateful to Professor Joseph Callaway for valuable discussions and to Dennis Ikenberry for very helpful advice on the calculation of the two-center integrals. The kind assistance of Miss Patricia Olinger in the preparation of the paper is also acknowledged.

APPENDIX A

In deriving Eqs. (16) or (22) for $\rho(\mathbf{r})$, we start with the OAO (17) or (20), respectively, and use the method developed by Slater and Koster.[35] The OAO given by Eq. (20) are not the symmetric Wannier functions of the antimony crystal structure. As they stand, they give rise to nonsymmetric energy bands which do not reflect the symmetry of reciprocal space. However, these OAO have resulted from a variation procedure as suggested by Koster,[40] and therefore, they are valid candidates for constructing symmetric Wannier functions for the crystal.

Our task is made simpler by using the fact that the OAO, given by Eq. (17) in the text, transform under point group operators in exactly the same way as do the basic atomic orbitals from which they are formed.[47] Because of this property, there is no mixing of the $a_s(\mathbf{r})$ or $a_z(\mathbf{r})$ hybridized OAO of (20) with the other members when they are acted on by the symmetry operations of the crystal. However, the $a_x(\mathbf{r})$ and $a_y(\mathbf{r})$ OAO of (20) are transformed into various linear combinations of one another under the crystal symmetry operations.

Following Slater and Koster, the symmetric Wannier functions of the crystal are

$$\begin{aligned}
a_s'(\mathbf{r})&=\textstyle\sum_{\mathbf{A}} N_s(\mathbf{A})a_s(\mathbf{r}-\mathbf{A})+\sum_{\mathbf{B}} N_s(\mathbf{B})a_s(\mathbf{r}-\mathbf{B}),\\
a_z'(\mathbf{r})&=\textstyle\sum_{\mathbf{A}} N_z(\mathbf{A})a_z(\mathbf{r}-\mathbf{A})+\sum_{\mathbf{B}} N_z(\mathbf{B})a_z(\mathbf{r}-\mathbf{B}),\\
a_x'(\mathbf{r})&=\textstyle\sum_{\mathbf{A}} [N_x'(\mathbf{A})a_x(\mathbf{r}-\mathbf{A})+N_y'(\mathbf{A})a_y(\mathbf{r}-\mathbf{A})]\\
&\quad+\textstyle\sum_{\mathbf{B}} [N_x'(\mathbf{B})a_x(\mathbf{r}-\mathbf{B})+N_y'(\mathbf{B})a_y(\mathbf{r}-\mathbf{B})],\\
a_y'(\mathbf{r})&=\textstyle\sum_{\mathbf{A}} [N_y^2(\mathbf{A})a_y(\mathbf{r}-\mathbf{A})N_x^2(\mathbf{A})a_x(\mathbf{r}-\mathbf{A})]\\
&\quad+\textstyle\sum_{\mathbf{B}} [N_y^2(\mathbf{B})a_y(\mathbf{r}-\mathbf{B})+N_x^2(\mathbf{B})a_x(\mathbf{r}-\mathbf{B})],
\end{aligned}\tag{A1}$$

where the $N_i(\mathbf{M})$ are derived[35] from the representations of the D_{3d}^5 space group of the antimony crystal structure, using the OAO given by Eq. (20) as the basis functions. What all this means is that the Wannier functions (A1) transform according to the one-dimensional irreducible representations of the D_{3d}^5 space group; and the energy bands acquired from these functions reflect all of the symmetry of reciprocal space. Another way of putting the above is to state that the basic set of OAO given by Eq. (20) of the text can be obtained from the properly symmetrized Wannier functions (A1) by a unitary transformation and vice versa.[35]

Using the above facts, Eqs. (A1) can be thus expressed as

$$a_j'(\mathbf{r})=\textstyle\sum_i [\sum_{\mathbf{A}} U_{ji}(\mathbf{A})a_i(\mathbf{r}-\mathbf{A})+\sum_{\mathbf{B}} U_{ji}(\mathbf{B})a_i(\mathbf{r}-\mathbf{B})],\tag{A2}$$

where $U^\dagger(\mathbf{M})U(\mathbf{N})\approx\delta_{\mathbf{MN}}I$. This latter property does not hold true rigorously in the Krönecker delta when $\mathbf{M}=\mathbf{A}$ and $\mathbf{N}=\mathbf{B}=\{\mathrm{NN}\}_{\mathbf{A}}$ (i.e., the nearest-neighbor B ions). However, if we consider the antimony lattice to be made up of two interpenetrating simple rhombohedral lattices which are coupled only through the process of symmetric orthonormalization [as typified by Eq. (17) of the text], then the above condition on the unitary matrices holds. This approximation is consistent with the further approximations which are made later on in the body of the text.

The charge density given by Eq. (6) in Sec. II shows that we can use the above properties to our advantage. Thus

$$\begin{aligned}
\rho(\mathbf{r})&=e\textstyle\sum_{\mathbf{M}}\sum_j|a_j'(\mathbf{r}-\mathbf{M})|^2=e\sum_{\mathbf{M}}\sum_j\sum_i(1+\delta_{is})^{1/2}[\sum_{\mathbf{A}} U_{ji}^\dagger(\mathbf{A})a_i^*(\mathbf{r}-\mathbf{A}-\mathbf{M})+\sum_{\mathbf{B}} U_{ji}^\dagger(\mathbf{B})a_i^*(\mathbf{r}-\mathbf{B}-\mathbf{M})]\\
&\quad\times\textstyle\sum_k(1+\delta_{ik})^{1/2}[\sum_{\mathbf{A}'} U_{jk}a_k(\mathbf{r}-\mathbf{A}'-\mathbf{M})+\sum_{\mathbf{B}'} U_{jk}(\mathbf{B}')a_k(\mathbf{r}-\mathbf{B}'-\mathbf{M})]\\
&=e\textstyle\sum_{\mathbf{M}}\sum_i\sum_k(1+\delta_{is})^{1/2}(1+\delta_{ik})^{1/2}\{\sum_{\mathbf{A}}\sum_{\mathbf{A}'}\delta_{ik}\delta_{\mathbf{AA}'}a_i^*(\mathbf{r}-\mathbf{A}-\mathbf{M})a_k(\mathbf{r}-\mathbf{A}'-\mathbf{M})\\
&\quad+\textstyle\sum_{\mathbf{B}}\sum_{\mathbf{B}'}\delta_{ik}\delta_{\mathbf{BB}'}a_i^*(\mathbf{r}-\mathbf{B}-\mathbf{M})a_k(\mathbf{r}-\mathbf{B}'-\mathbf{M})\}.
\end{aligned}$$

We have used the condition $\sum_j U_{ji}^\dagger(A)U_{jk}(A')=\delta_{ik}\delta_{\mathbf{AA}'}$ and the condition $\sum_j U_{ji}^\dagger(\mathbf{A})U_{jk}(\mathbf{B})=0$ for all $\mathbf{A}$, $\mathbf{B}$. The factors $(1+\delta_{is})^{1/2}$ and $(1+\delta_{ik})^{1/2}$ are necessary assuming that both the bonding and antibonding s states are doubly occupied. For indices $i=x$, y, and z, we assume only the bonding state is doubly occupied. Carrying out the summations implied above, we get

$$\rho(\mathbf{r})=e\textstyle\sum_{\mathbf{M}}\sum_i(1+\delta_{is})\{\sum_{\mathbf{A}}|a_i(\mathbf{r}-\mathbf{A}-\mathbf{M})|^2+\sum_{\mathbf{B}}|a_i(\mathbf{r}-\mathbf{B}-\mathbf{M})|^2\}.\tag{A3}$$

When we consider only the terms $\mathbf{M}=\mathbf{A}=0$ and $\mathbf{B}=\{\mathrm{NN}\}_{\mathbf{A}}$, Eq. (16) of the text follows.

APPENDIX B: ROTATION OPERATORS FOR OVERLAP INTEGRALS

There is very little consistency in the literature in choice of axes and rotation directions for which one defines rotation matrices. Rather than use the general machinery of group theory, we will employ only that

[47] J. C. Slater and G. F. Koster, Phys. Rev. 94, 1498 (1954).

simpler theory necessary for finding those particular elements of interest in this paper.

We first consider a counterclockwise rotation ϕ_R about the z axis followed by a counterclockwise rotation θ_R about the new y axis. The first operation is

$$\begin{pmatrix} x'' \\ y'' \\ z'' \end{pmatrix} = \begin{pmatrix} \cos\phi_R & \sin\phi_R & 0 \\ -\sin\phi_R & \cos\phi_R & 0 \\ 0 & 0 & 1 \end{pmatrix} \begin{pmatrix} x \\ y \\ z \end{pmatrix}, \quad \text{(B1)}$$

and the second is

$$\begin{pmatrix} x' \\ y' \\ z' \end{pmatrix} = \begin{pmatrix} \cos\theta_R & 0 & -\sin\theta_R \\ 0 & 1 & 0 \\ \sin\theta_R & 0 & \cos\theta_R \end{pmatrix} \begin{pmatrix} x'' \\ y'' \\ z'' \end{pmatrix}. \quad \text{(B2)}$$

Combining these two operations, we get

$$\begin{pmatrix} x' \\ y' \\ z' \end{pmatrix} = \begin{pmatrix} \cos\phi_R\cos\theta_R & \sin\phi_R\cos\theta_R & -\sin\theta_R \\ -\sin\phi_R & \cos\phi_R & 0 \\ \cos\phi_R\sin\theta_R & \sin\phi_R\sin\theta_R & \cos\theta_R \end{pmatrix} \begin{pmatrix} x \\ y \\ z \end{pmatrix}. \quad \text{(B3)}$$

Our objective, however, is to expand the coordinates (x,y,z) in terms of the rotated coordinates (x',y',z') and therefore, we need the inverse of the above operation.

$$\begin{pmatrix} x \\ y \\ z \end{pmatrix} \begin{pmatrix} \cos\phi_R\cos\theta_R & -\sin\phi_R & \cos\phi_R\sin\theta_R \\ =\sin\phi_R\cos\theta_R & \cos\phi_R & \sin\phi_R\sin\theta_R \\ -\sin\theta_R & 0 & \cos\theta_R \end{pmatrix} \begin{pmatrix} x' \\ y' \\ z' \end{pmatrix}. \quad \text{(B4)}$$

These equations can now be applied to the orbitals and operator of interest.

The orbitals are cast as px, py, and pz, so that equations (B4) as they are, give the desired transformation. Hence

$$\begin{pmatrix} p_x \\ p_y \\ p_z \end{pmatrix} = \begin{pmatrix} \cos\phi_R\cos\theta_R & -\sin\phi_R & \cos\phi_R\sin\theta_R \\ \sin\phi_R\cos\theta_R & \cos\phi_R & \sin\phi_R\sin\theta_R \\ -\sin\theta_R & 0 & \cos\theta_R \end{pmatrix} \begin{pmatrix} p_x' \\ p_y' \\ p_z' \end{pmatrix}. \quad \text{(B5)}$$

We next make use of the forms

$$\begin{aligned} p_x' &= (1/\sqrt{2})(f_{51}(r)/r)(Y_1^1(\theta_1'\phi_1') + Y_1^{-1}(\theta_1'\phi_1')), \\ p_y' &= (1/\sqrt{2})(f_{51}(r)/r)(-iY_1^1(\theta_1'\phi_1') + iY_1^{-1}(\theta_1'\phi_1')), \\ p_z' &= (f_{51}(r)/r)Y_1^0(\theta_1'\phi_1'). \end{aligned} \quad \text{(B6)}$$

Substituting (B6) into (B5) gives, for example,

$$\begin{aligned} p_x = {} & (f_{51}(r)/r) \\ & \times\{[(1/\sqrt{2})(\cos\phi_R\cos\theta_R + i\sin\phi_R)]Y_1^1(\theta_1'\phi_1') \\ & + \cos\phi_R\sin\theta_R Y_1^0(\theta_1'\phi_1') \\ & + [(1/\sqrt{2})(\cos\phi_R\cos\theta_R - i\sin\phi_R)]Y_1^{-1}(\theta_1'\phi_1'). \end{aligned} \quad \text{(B7)}$$

We can define the coefficients preceding each spherical harmonic using the usual symbol $D_{iM}^L(\theta_R,\phi_R,\psi_R)$, where θ_R and ϕ_R are our choices of Euler angles and where $\psi_R=0$. In this present example $L=1$, $i=px$, py, pz (or x, y, z) and $M=0,\pm1$. Using the above symbol, the px orbital can conveniently be expressed as

$$p_x = (f_{51}(r)/r)\sum_{M=-1}^{1} D_{p_xM}^1(\theta_R,\phi_R,0)Y_1^M(\theta_1'\phi_1') \quad \text{(B8)}$$

with similar expressions for py and pz.

The operator of interest is of the form $(1/r^3)Y_{20}(\theta,\phi)$. The substitution of (B4) in this expression can be made after expressing $Y_{20}(\theta,\phi)$ as a function of (x,y,z). Hence

$$r^{-3}Y_2^0(\theta,\phi) = (5/16\pi)^{1/2}(3z^2-r^2)/r^5 \quad \text{(B9)}$$

and, by substitution,

$$\begin{aligned} & r^{-3}Y_2^0(\theta,\phi) \\ & \quad = (5/16\pi)^{1/2}3(-x'\sin\theta_R + z'\cos\theta_R)^2 - r'^2/r'^5. \end{aligned} \quad \text{(B10)}$$

When the above expression is expanded and is re-expressed as spherical harmonics, one gets

$$\begin{aligned} r^{-3}Y_2^0(\theta,\phi) = {} & [(6/4)\sin^2\theta_R](1/r^3)Y_2^2(\theta',\phi') \\ & + [-(6/2)\sin\theta_R\cos\theta_R](1/r'^3)Y_2^1(\theta',\phi') \\ & + [1-\tfrac{3}{2}\sin^2\theta_R](1/r'^3)Y_2^0(\theta',\phi') \\ & + [-(6/2)\sin\theta_R\cos\theta_R](1/r'^3)Y_2^{-1}(\theta',\phi') \\ & + [(6/4)\sin^2\theta_R](1/r'^3)Y_2^{-2}(\theta',\phi'). \end{aligned} \quad \text{(B11)}$$

The expressions in the brackets can be defined in terms of the $D_{iM}^L(\theta_R,\phi_R,\psi_R)$, and the expansion becomes

$$\begin{aligned} & r^{-3}Y_2^0(\theta,\phi) \\ & \quad = (1/r'^3)\sum_{M=-2}^{2} D_{0M}^2(\theta_R,\phi_R,0)Y_2^M(\theta',\phi'). \end{aligned} \quad \text{(B12)}$$

This completes the process of re-expressing the orbitals and the operator in terms of the harmonics defined relative to the rotated coordinate systems.